Economic Geology, v. 100, pp. 905–934

Magmatic and Hydrothermal Chronology of the Giant Río Blanco Porphyry Copper Deposit, Central Chile: Implications of an Integrated U-Pb and $^{40}Ar/^{39}Ar$ Database

Katja Deckart,†

Departamento de Geología, Universidad de Chile, Plaza Ercilla 803, Casilla 13518, Santiago, Chile

Alan H. Clark,

Department of Geological Sciences and Geological Engineering, Queen's University, Kingston, Ontario, Canada K7L 3N6

Celso Aguilar A., Ricardo Vargas R.,

Corporación Nacional del Cobre de Chile, División Andina, Sta. Teresa 513, Los Andes, Chile

Alfredo Bertens, N.,

Corporación Nacional del Cobre de Chile, Exploraciones y Mineras S.A., Apoquindo 4775, Santiago, Chile

James K. Mortensen,

Pacific Centre for Isotopic and Geochemical Research, Department of Earth and Ocean Sciences, University of British Columbia, 6339 Stores Road, Vancouver, British Columbia, Canada V6T 1Z4

and Mark Fanning

Research School of Earth Sciences, Australian National University, Canberra, ACT 0200, Australia

Abstract

The history of hypabyssal intrusion and hydrothermal activity in the northeastern and central parts of the behemothian (sensu Clark, 1993) Río Blanco-Los Bronces porphyry copper-molybdenum deposit is clarified on the basis of integrated U-Pb and $^{40}Ar/^{39}Ar$ geochronology. Isotope dilution thermal ion mass spectrometry (ID-TIMS) U-Pb dates for zircon separates and ID-TIMS and sensitive high resolution ion microprobe (SHRIMP) dates for single zircon grains in pre-, syn- and late-mineralization volcanic and intrusive host rocks in the Río Blanco, Don Luis, and Sur-Sur mining sectors provide a temporal framework for interpretation of incremental-heating and spot-fusion $^{40}Ar/^{39}Ar$ dates for, respectively, magmatic biotite and hydrothermal biotite, muscovite, and orthoclase.

The ore deposit is hosted in part by 16.77 ± 0.25 to 17.20 ± 0.05 (2σ) Ma andesitic volcanic strata of the Farellones Formation, but the major host rocks are units of the San Francisco batholith, including the 11.96 ± 0.40 Ma Río Blanco granodiorite (mine terminology), the 8.40 ± 0.23 Ma Cascada granodiorite, and the 8.16 ± 0.45 Ma diorite. Hypabyssal dacitic intrusions (late porphyries) emplaced into the batholith yield $^{206}Pb/^{238}U$ ID-TIMS dates ranging from 6.32 ± 0.09 Ma (quartz monzonite porphyry), through 5.84 ± 0.03 Ma (feldspar porphyry) to 5.23 ± 0.07 Ma (Don Luis porphyry). The late-mineralization Río Blanco dacite plug yields a SHRIMP zircon age of 4.92 ± 0.09 Ma.

The $^{40}Ar/^{39}Ar$ plateau ages for phenocrystic biotites in quartz monzonite porphyry, feldspar porphyry, and Don Luis porphyry, as well as the preore diorite, range only from 5.12 ± 0.07 to 4.57 ± 0.06 Ma. All are significantly younger than the corresponding zircons and exhibit no correlation with intrusive sequence. The $^{40}Ar/^{39}Ar$ ages for hydrothermal biotite and orthoclase veins within the San Francisco batholith units fall in a narrow interval from 5.32 ± 0.27 to 4.59 ± 0.11 Ma. Hydrothermal sericites (muscovite), one associated with chalcopyrite, yielded spot-fusion ages of 4.40 ± 0.15 Ma (Río Blanco granodiorite hosted) and 4.37 ± 0.06 Ma (Don Luis porphyry hosted). Comparison with the ID-TIMS and SHRIMP zircon ages indicates that most of the $^{40}Ar/^{39}Ar$ ages, even 95 percent plateaus, do not record initial magmatic cooling or hydrothermal alteration-mineralization events, evidence for quasipervasive reheating to at least 300ºC by successive intrusions. Published Re-Os ages for two molybdenite samples range from 5.4 to 6.3 Ma and overlap extensively with the zircon U-Pb ages for the late porphyries. They imply that Cu-Mo mineralization overlapped temporally with the emplacement of, at least, quartz monzonite porphyry and feldspar porphyry units of the late porphyry suite and was, therefore, contemporaneous with the rise of dacitic melts to subvolcanic levels. Hydrothermal activity is inferred to have continued until 4.37 ± 0.06 Ma, following intrusion of the Don Luis porphyry and the early stages of emplacement of the Río Blanco dacite plug complex. Hypogene Cu-Mo mineralization therefore probably persisted for 2 m.y. The geochronologic data do not resolve whether ore formation was continuous or episodic, but the observed crosscutting relationships between intensely altered and mineralized country rocks and less altered and mineralized late porphyry bodies support a model in which the ascent of metal-rich brines from an unexposed zone of the parental magma chamber was periodically stimulated by magma perturbation and hypabyssal intrusion.

† Corresponding author: e-mail, kdeckart@cec.uchile.cl

0361-0128/05/3528/905-30 $6.00

Introduction

Considerable discussion has been devoted to the petrogenetic, geochemical, and tectonic processes responsible for the formation of the few outsize ore deposits which account for much of global metal production (e.g., Whiting et al., 1993). In the field of porphyry copper-molybdenum mineralization, it has been widely assumed that giant deposits are the products of exceptionally protracted and/or unusually multistage histories of alteration-mineralization, although the early K-Ar database did not convincingly support this model (e.g., Clark, 1993). The introduction of incremental-heating $^{40}Ar/^{39}Ar$ dating techniques, particularly those involving laser fusion, resulted in a significant increase in analytically precise data for hydrothermal alteration and ore assemblages (e.g., Clark et al., 1998; Reynolds et al., 1998; Gustafson et al., 2001). However, given the relatively low Ar retention temperatures of several key alteration minerals (e.g., ca. 310ºC for biotite: Harrison et al., 1985; 280º–290ºC for alunite: Love et al., 1998), it is recognized that studies integrating $^{40}Ar/^{39}Ar$ geochronology with U-Pb isotope dilution thermal ion mass spectrometry (ID-TIMS) dating of zircon fractions, or ID-TIMS and sensitive high resolution ion microprobe (SHRIMP) dating of individual zircon grains in the igneous rocks associated with mineralization, are likely to provide the most rigorous constraints on magmatic-hydrothermal chronology (e.g., Richards et al., 1999). This approach also permits assessment of an alternative model for supergiant porphyry systems, originally stimulated by the geochronologic research of Reynolds et al. (1998) at Chuquicamata, i.e., that the largest such deposits may be products of distinct, superimposed magmatic-hydrothermal events.

In the present contribution, we integrate new U-Pb zircon data for igneous bodies with multistep $^{40}Ar/^{39}Ar$ age spectra obtained by laser-induced step heating of separates and spot-fusion $^{40}Ar/^{39}Ar$ ages for alteration and vein minerals to clarify the temporal relationships in one of the largest known porphyry Cu-Mo systems, the Río Blanco-Los Bronces deposit, V. región, Chile. The geology of this multicentered behemoth has been extensively described (e.g., Warnaars et al., 1985; Serrano et al., 1996; Skewes et al., 2003) and, on a regional scale, models have been advanced for the metallogenic relationships of this and allied Neogene mineral deposits in the Andean Principal Cordillera of central Chile and contiguous Argentina (e.g., Skewes and Stern, 1995; Kay et al., 1999; Kay and Mpodozis, 2001; Skewes et al., 2002). An early Pliocene age for mineralization has been accepted since the work of Quirt et al. (1971) and Quirt (1972), and the youth of the deposit renders it ideal for precise geochronologic research. However, the conventional K-Ar ages reported in that study, 4.03 ± 0.19 and 4.73 ± 0.16 Ma (2σ errors; ages recalculated to the decay constants recommended by Steiger and Jäger, 1977), were for ostensibly phenocrystic biotites selected by R.H. Sillitoe from volcanic and intrusive porphyry bodies which have generally been considered to have postdated the main episodes of Cu and Mo mineralization. Although the geochronologic database has since considerably expanded (e.g., in Serrano et al., 1996), it includes numerous whole-rock K-Ar ages of problematic significance, and few of the ages for mineral separates have been formally documented in accessible publications. The duration of economic ore formation is therefore poorly delimited, and its geodynamic context thus remains uncertain. Our study focused on the eastern, Río Blanco, portion of the deposit but is relevant to the entire hydrothermal system. It includes the first ID-TIMS and SHRIMP U-Pb ages of zircons from igneous units in this area and the first analytically precise $^{40}Ar/^{39}Ar$ age spectra for magmatic and hydrothermal minerals.

Geologic Relationships

Operated since 1971 by the Andina Division of CODELCO-Chile, the Río Blanco mine incorporates the central and southern sectors of an extensive hydrothermal complex (Fig. 1), the northwesterly third of which is exploited by the Los Bronces mine of Compañía Minera Disputada de Las Condes, since 2002 a subsidiary of Anglo American plc. The deposit occupies a ca. 15-km^2 area elongated northwest-southeast (Fig. 2). The CODELCO-Andina operations comprise

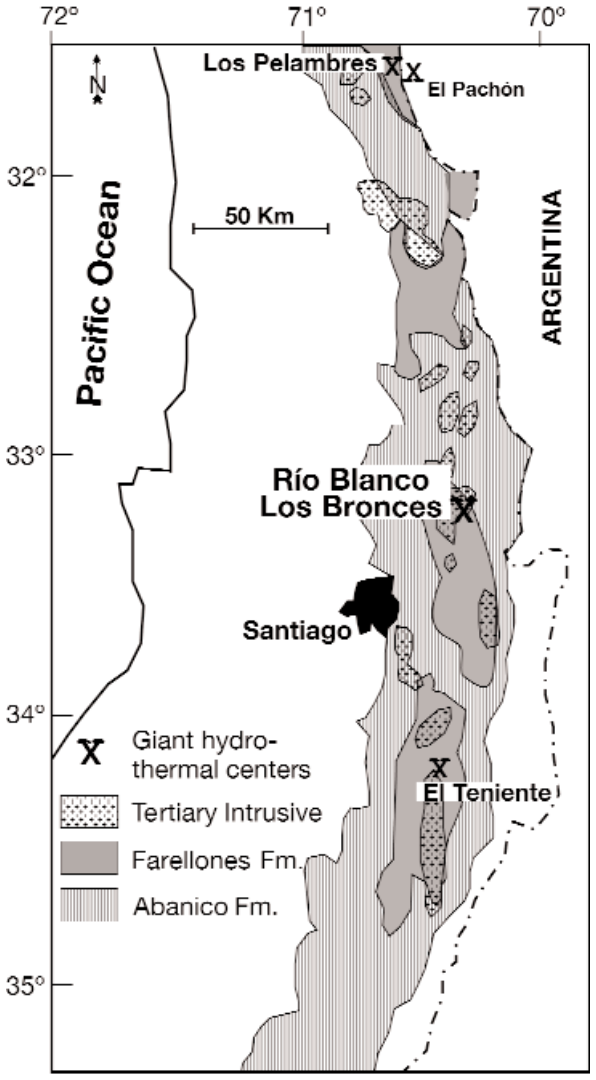

Fig. 1. Simplified regional geologic map of the Late Tertiary magmatic belt, Central Chile, showing locations of the Río Blanco-Los Bronces deposit and other major Mio-Pliocene porphyry Cu-Mo deposits. Modified from Serrano et al. (1996).

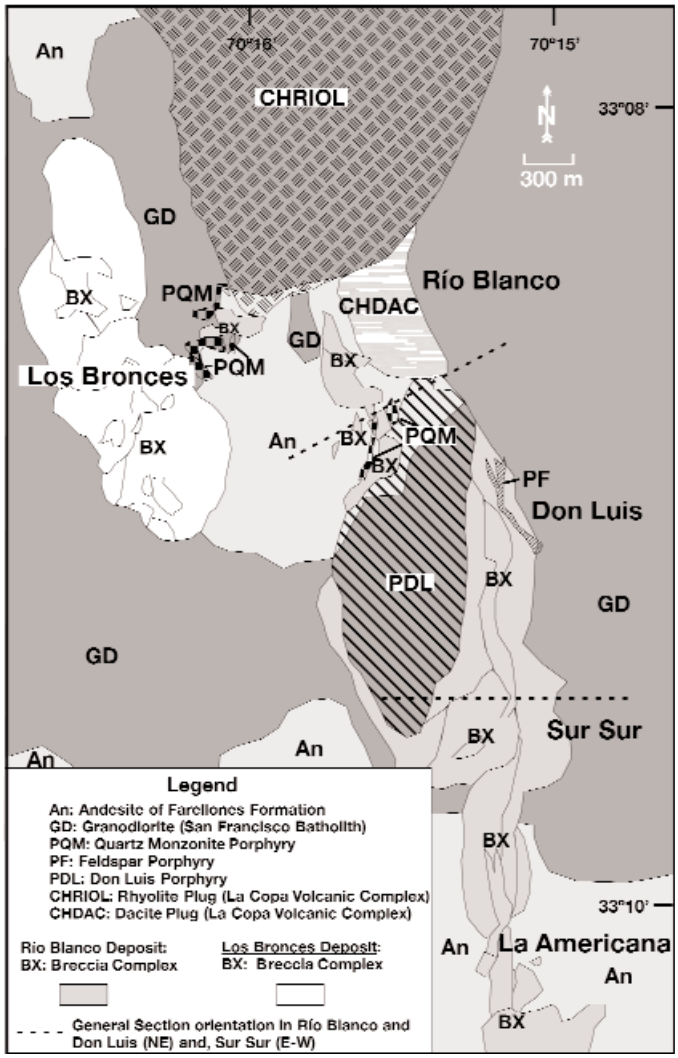

FIG. 2. Simplified geologic map of the Río Blanco-Los Bronces porphyry copper deposit. Modified from Vargas et al. (1999) and Frikken et al. (2005). General section orientations for Río Blanco and Don Luis (N62°E; Fig. 3A-B) and Sur-Sur (E-W; Fig. 3C) sectors are shown. The quartz monzonite, feldspar, and Don Luis porphyry intrusions are known collectively as the late porphyries.

the Río Blanco underground mine, underlying the original Andina block-cave mine and extending southward into the Don Luis sector (Fig. 2) and, farther to the south-southeast, the Sur-Sur open pit. These operations have daily productions of, respectively, ca. 15,000 t at 1.0 percent Cu and 20,000 t at 1.5 percent Cu, while the Los Bronces open pit yields 37,000 t/d at 1.21 percent Cu. Aggregate production from the two mines in 2001 was 435,900 t of fine Cu and 7324 t of Mo in concentrates. Although supergene oxidation and sulfide enrichment have locally resulted in significant upgrading, the combined Río Blanco-Los Bronces center contains over 7.2 Gt of hypogene sulfide assemblages with an average grade of 0.82 percent Cu, at a cut-off grade of 0.5 percent Cu (CODELCO Andina División, pers. commun., 2002). The Mo resource exceeds 8×10^5 t. As at El Teniente (Fig. 1; cf. Skewes et al., 2002; Cannell et al., 2005), the Cu-Mo mineralization is hosted by both stockwork vein systems and hydrothermal breccias.

Local geology

The geology of the Río Blanco-Los Bronces porphyry center (Fig. 2) has been summarized by Serrano et al. (1996), drawing on numerous inhouse reports and published data, including Warnaars et al.'s (1985) description of the Los Bronces mine. Vargas et al. (1999) reviewed the mineralized breccias in both the Río Blanco and Los Bronces sectors, while Skewes et al. (2003) provided a detailed description of the Donoso breccia orebody in the Los Bronces mine. (N.B. As in many long-established mines, igneous bodies and hydrothermal centers have assumed traditional names which form the basis for local correlation but which are not necessarily genetically reliable: this usage is followed herein, employing lower case throughout for nonproper names).

The district- and regional-scale settings of the deposit have been addressed by, among others, Skewes and Stern (1995, 1996), Kay et al. (1999), Kay and Mpodozis (2001, 2002), Skewes et al. (2002) and Hollings et al. (2005).

Northeast-southwest (N62°E) sections through the Río Blanco and Don Luis sectors are shown in Figure 3A and B, respectively, and an east-west premining section through the Sur-Sur sector in Figure 3C. The host rocks of the breccia and stockwork mineralization include subhorizontal, dominantly andesitic, subaerial flows and volcaniclastics, which have been assigned to either the Farellones Formation (Stambuk et al., 1985; Warnaars et al., 1985) or the older Abanico Formation (Rivano et al., 1990), both considered to be of early or middle Miocene age (Vergara et al., 1988). However, much of the ore is hosted by intermediate to silicic granitoid units constituting the western margin of the younger San Francisco batholith, of inferred early or middle Miocene age. Hydrothermal alteration of these country rocks, both potassic and, less intensely, sericitic, has caused uncertainty in the interpretation of the available K-Ar age data, particularly for the San Francisco granitoids (Serrano et al., 1996).

The hydrothermal history of the Río Blanco-Los Bronces complex is considered to have commenced with development of an extensive alteration system, largely in granitoid rocks, characterized by actinolite-magnetite ± clinopyroxene ± titanite ± plagioclase assemblages, with mineralogically similar veins and breccia cements (Skewes et al., 1994, 2003). This association, involving Fe metasomatism, is similar in many respects to that documented in the Island Copper porphyry Cu-Mo-Au deposit, British Columbia, by Arancibia and Clark (1995) and shares its paucity or lack of sulfides. The earliest economic mineralization event postulated by Serrano et al. (1996) coincided with intense potassic alteration, dominantly biotitic, of both andesites and granitoid rocks, centered on the Río Blanco sector. Biotite ± magnetite ± sulfides ± K-feldspar alteration was associated with the development of a stockwork of mineralogically similar veins, in which chalcopyrite is accompanied by lesser bornite, pyrite and molybdenite. The Río Blanco breccia complex (e.g., Fig. 3A), closely associated with the K silicate alteration, comprises swarms of intensely mineralized, vertically elongated, kidney-shaped bodies in which the matrix assemblages range from biotite dominant (so-called magmatic breccia) to tourmaline rich, in both cases

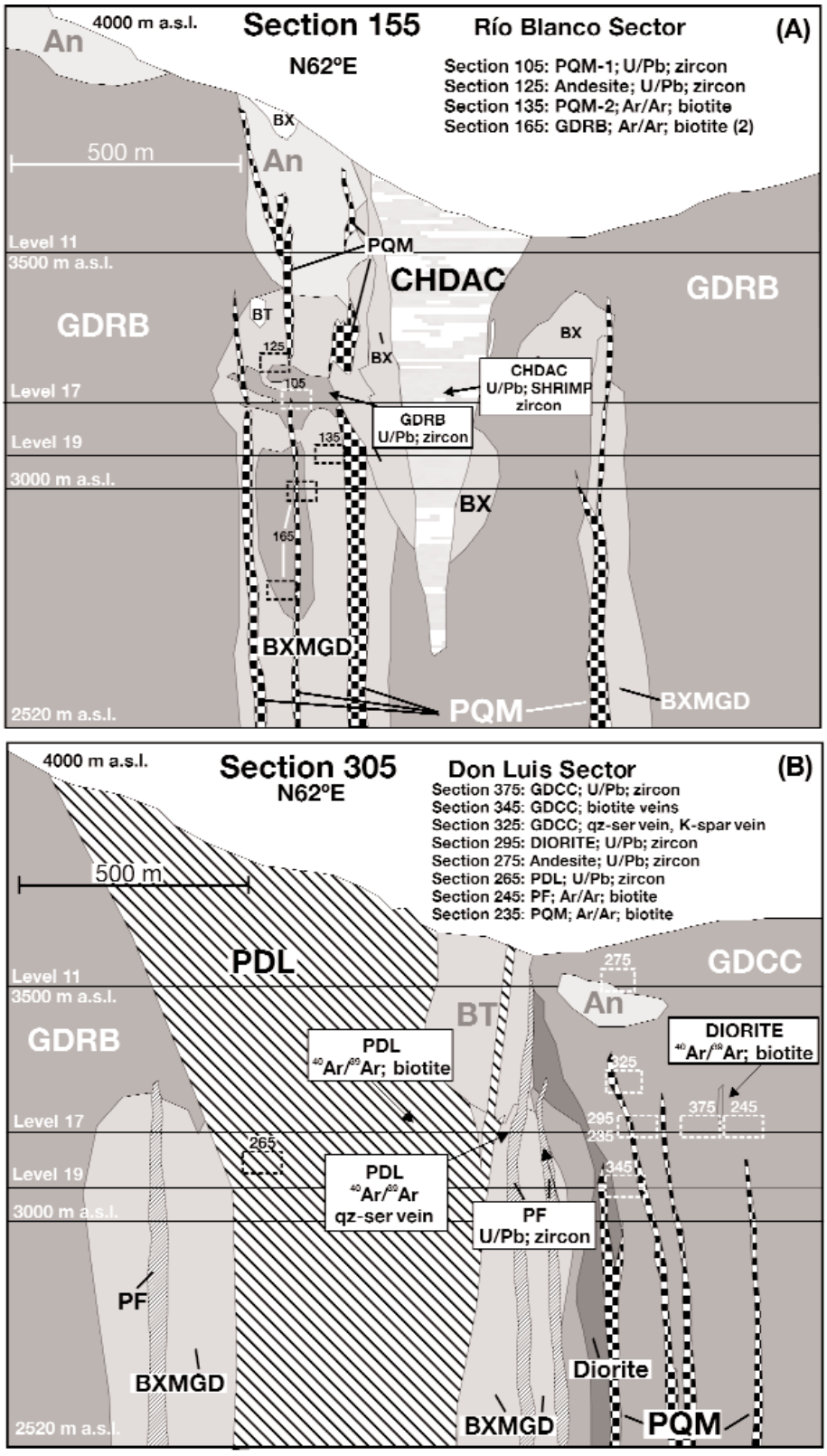

FIG. 3. A. Cross section 155 (N62°E) of the Río Blanco sector with sample locations and projected locations of samples from parallel sections 105, 125, 135, and 165. B. Cross section 305 (N62°E) of the Don Luis sector with sample locations and projected locations of samples from parallel sections 325, 345, 375, 295, 275, 265, 245, and 235. C. Cross section 50 (E-W) of the Sur-Sur sector with sample location. Section numbers refer to local mine coordinates, starting in the Río Blanco and Don Luis sectors at 05 and increasing at units of ten to the north and, in the Sur-Sur sector, starting at 00 and increasing to the north at intervals of 10. The sections are 60 m apart.

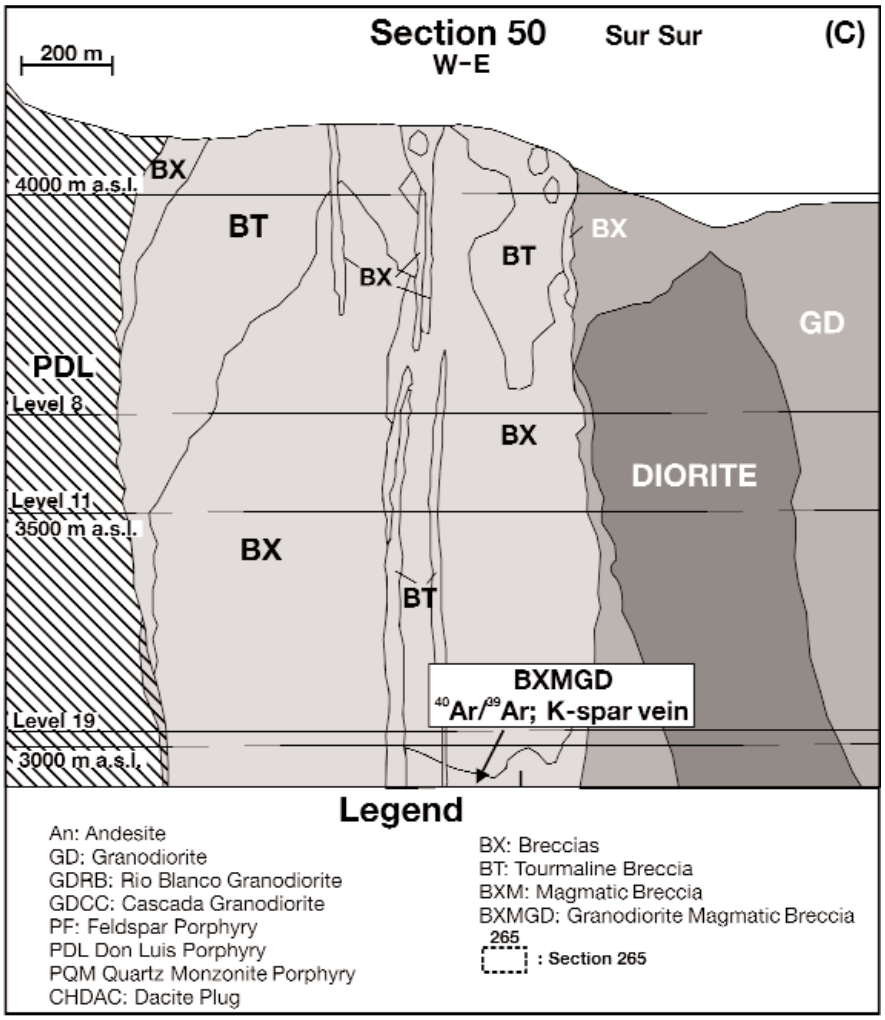

FIG. 3. *(Cont.)*

with varying proportions of quartz, anhydrite and sulfides, including chalcopyrite, bornite, molybdenite, and minor pyrite. Fluid inclusion microthermometric data (Kusakabe et al., 1990) yield emplacement pressures equivalent to depths of over 3 km, but the roots of the breccia bodies are not exposed.

K-Ar whole-rock and mineral data have been interpreted as evidence for a later episode of intense Cu and Mo mineralization, represented by a cluster of breccias (e.g., Serrano et al. 1996), extensively mined in the Sur-Sur sector (Figs. 2, 3C), in which the matrix comprises tourmaline and sulfides, associated in lower grade zones with subordinate quartz, chlorite, sericite, anhydrite, specularite, and, at depth, biotite. The Los Bronces mine (Fig. 2) exploits comparable orebodies (Warnaars et al., 1985; Skewes et al., 2003). The fluids responsible for this apparent second major stage of Cu-Mo emplacement were similar to those of the earlier stage, i.e., high-temperature (>450ºC), highly saline, boiling, and dominated by magmatic rather than meteoric sources. Skewes and Holmgren (1993) demonstrated that the major Donoso breccia in the Los Bronces mine (Fig. 2), hosted by a granodioritic unit of the San Francisco batholith, formed within a few hundred meters of surface, implying (Serrano et al., 1996, p. 126) "significant erosional unroofing of this pluton prior to emplacement of the breccia." Hydrothermal alteration associated with this second phase of ore formation was largely represented by variable proportions of tourmaline, sulfides, quartz, chlorite, sericite and anhydrite, concentrated in clasts and matrix within the breccias.

The mineralized potassic alteration zone, early breccias, and tourmaline breccias have been intruded by large hypabyssal dacitic-and-rhyolitic bodies, known collectively as the late porphyries. Vergara and Latorre (1984) assigned these and their extrusive equivalents to the Río Blanco volcanic complex, whereas Blondel et al. (1988) grouped them as the Río Blanco formation. Intrusive units distinguished by mine geologists include (Fig. 2) quartz monzonite porphyry (pórfido quarzo monzonitico), feldspar porphyry, Don Luis porphyry, and the downward-tapering (Fig. 3A) Río Blanco dacite plug. Associated rhyolitic intrusive (rhyolite plug) and less extensive eruptive bodies, which dominate outcrops at the northern limit of the deposit, are assigned to the La Copa volcanic complex (Fig. 2). The dacite plug unit is extensively sericitized, particularly along its intensely brecciated western margin (Fig. 3A). In contrast, the La Copa volcanic complex,

including the rhyolite plug, is largely unaltered and is considered as postore. The weak (≤0.5% Cu) mineralization hosted by the late porphyry bodies, including intermediate- to high-sulfidation Cu-Mo-Pb-Zn-As vein systems, is traditionally ascribed to remobilization of earlier assemblages (Serrano et al., 1996), a process envisaged to have locally enhanced preexisting Cu grades. In a detailed study of the eastern part of the deposit, Frikken (2004) has shown that feldspar porphyry in the Río Blanco sector contains clasts of mineralized magmatic breccia, but he also documented textural relationships suggesting that this intrusive unit was emplaced approximately contemporaneously with the tourmaline breccia in the Don Luis sector. Further, three bodies of rock flour-cemented breccia in the Sur-Sur sector entrain blocks of Don Luis porphyry.

Previous geochronologic data

A summary of the extant geochronologic database is provided herein as Table 1, which includes K-Ar, $^{40}Ar/^{39}Ar$ incremental-heating, and Re-Os molybdenite ages. Whereas no age determinations have been reported for the volcanic rocks of the immediate mine area, the San Francisco batholith has been extensively studied (e.g., in Serrano et al., 1996). An early Miocene age for the batholith is supported by a $^{40}Ar/^{39}Ar$ biotite plateau age of 14.82 ± 0.12 Ma for a sample collected 10 km south of the Los Bronces mine. Younger $^{40}Ar/^{39}Ar$ ages have been ascribed to resetting by a postulated initial intrusive or alteration event at 5.4 Ma, based on $^{40}Ar/^{39}Ar$ plateau ages for a K-feldspar vein and dispersed K-feldspar single grains. However, an even younger $^{40}Ar/^{39}Ar$ biotite inverse isochron age of 4.58 ± 0.16 Ma from the same drill core section has been interpreted as recording a second thermal event affecting only the biotite.

The mineralized assemblages have yielded K-Ar ages interpreted as evidence that the magmatic breccia in the Río Blanco sector was emplaced at ca. 7.3 Ma, whereas the Sur-Sur tourmaline breccia formed at ca. 5.1 Ma (Table 1). However, the majority of these ages were determined on whole-rock samples, many clearly heterolithologic. The significance of these data is therefore uncertain, particularly with regard to the tourmaline breccia, which incorporates clasts with preexisting alteration-mineralization assemblages and a matrix rich in tourmaline, a mineral known to incorporate excess Ar. $^{40}Ar/^{39}Ar$ ages of 4.61 ± 0.04 and 4.23 ± 0.04 Ma reported for, respectively, biotite and K-feldspar from the Río Blanco magmatic breccias (Table 1) are both much younger than the corresponding K-Ar age for the whole rock, which presumably comprised matrix and clasts. Two recently obtained $^{40}Ar/^{39}Ar$ ages on biotite cement and sericite-rich whole rock for a mineralized breccia body in the Sur-Sur quadrant (Frikken et al., 2005) support the younger brecciation event previously recognized for this sector. The late porphyries have been extensively dated (Table 1), with apparent emplacement ages ranging from 5.20 ± 0.12 Ma ($^{40}Ar/^{39}Ar$) to 4.03 ± 0.19 Ma (K-Ar).

The above database is in permissive agreement with the conclusions of Quirt et al. (1971) and Sillitoe (1988) that Cu-Mo ore formation at Río Blanco-Los Bronces took place in the Pliocene. It is, however, both significant and paradoxical that the majority of the $^{40}Ar/^{39}Ar$ ages determined for hydrothermal minerals directly associated with Cu-Mo mineralization are

TABLE 1. Previous Geochronologic Data Related to the Río Blanco-Los Bronces Porphyry Copper Deposit, Central Chile

Rock unit	Rock type	Dated Material	Method	Age (Ma) ± 2σ	References
Farellones Formation	Pyroxene andesite: not in the mine area	Plagioclase	K-Ar	18.5 ± 0.2	Vergara and Drake (1978)
	Rhyolite tuff: not in the mine area	Plagioclase	K-Ar	17.3 ± 0.3	Vergara and Drake (1978)
San Francisco pluton	Quartz monzonite, Los Piches	Biotite	$^{40}Ar/^{39}Ar$	14.82 ± 0.12 (PA)	F. Munizaga, unpub. report (1994)[1]
	Hornblende diorite, Los Bronces	Hornblende	K-Ar	18.5 ± 1.7 (1σ?)	Warnaars et al. (1985)
	Hornblende diorite, Los Bronces	Biotite	K-Ar	12.0 ± 0.5 (1σ?)	Warnaars et al. (1985)
	Quartz monzonite, Los Bronces	Biotite	K-Ar	11.3 ± 0.4 (1σ?)	Warnaars et al. (1985)
	Granodiorite, Río Blanco	Biotite	K-Ar	11.7 ± 0.9	SERNAGEOMIN unpub. report (1988) [1]
	Granodiorite, Los Bronces	Plagioclase	K-Ar	8.6 ± 0.1	Vergara and Drake (1979)
	Granodiorite, Los Bronces	Hornblende	K-Ar	8.6 ± 0.9	Warnaars et al. (1985)
	Granodiorite, Los Bronces	Plagioclase	K-Ar	8.4 ± 0.2	Vergara and Drake (1979)
	Granodiorite, Los Bronces	Biotite	K-Ar	7.9 ± 0.4 (1σ?)	Warnaars et al. (1985)
	Mineralized granodiorite, Los Bronces	Plagioclase	K-Ar	7.4 ± 0.1	Vergara and Drake (1979)
	Sericitized quartz monzonite	Sericite	K-Ar	5.2 ± 0.3 (1σ?)	Warnaars et al. (1985)
	Granodiorite Río Blanco	Biotite	$^{40}Ar/^{39}Ar$	4.58 ± 0.16 [3]	A. Skewes, unpub. report (1997) [2]
	Granodiorite Río Blanco	K-feldspar	$^{40}Ar/^{39}Ar$	5.47 ± 0.08 (PA)	A. Skewes, unpub. report (1997) [2]
	Granodiorite Río Blanco	K-feldspar vein	$^{40}Ar/^{39}Ar$	5.40 ± 0.05 (PA)	A. Skewes, unpub. report (1997) [2]
Breccia complex	Magmatic breccia, Río Blanco	Whole rock	K-Ar	7.3 ± 0.7	SERNAGEOMIN unpub. report (1988) [1]
	Tourmaline breccia, Río Blanco	Whole rock	K-Ar	7.1 ± 0.8	SERNAGEOMIN unpub. report (1988) [1]
	Tourmaline breccia, La Americana	Whole rock	K-Ar	5.9 ± 0.2	Spröhnle (1988)
	Paloma breccia, Sur-Sur	Whole rock	K-Ar	5.2 ± 0.2	Spröhnle (1988)
	Tourmaline breccia, Sur-Sur	Whole rock	K-Ar	5.3 ± 0.2	Spröhnle (1988)

TABLE 1. *(Cont.)*

Rock unit	Rock type	Dated Material	Method	Age (Ma) ± 2σ	References
		Whole rock	K-Ar	5.1 ± 0.2	Spröhnle (1988)
	Monolito breccia, Sur-Sur	Whole rock	K-Ar	5.2 ± 0.4	SERNAGEOMIN unpub. report (1988) [1]
	Magmatic breccia Río Blanco	Biotite	$^{40}Ar/^{39}Ar$	4.61 ± 0.04 [4]	F. Munizaga, unpub. report (1994) [1]
	Magmatic breccia Río Blanco	K-feldspar	$^{40}Ar/^{39}Ar$	4.23 ± 0.04 (PA)	F. Munizaga, unpub. report (1994) [1]
	Breccia Los Machos, Los Bronces	Matrix biotite	$^{40}Ar/^{39}Ar$	14.14 ± 0.06 (PA)	A. Skewes, unpub. report (1997) [2]
		Matrix hornblende	$^{40}Ar/^{39}Ar$	14.15 ± 0.34 (PA)	A. Skewes, unpub. report (1997) [2]
	Breccia north of Los Machos Sector,	Matrix biotite	$^{40}Ar/^{39}Ar$	8.49 ± 0.06 (PA)	A. Skewes, unpub. report (1997) [2]
	Los Bronces	Matrix K-feldspar	$^{40}Ar/^{39}Ar$	6.68 ± 0.54 [4]	A. Skewes, unpub. report (1997) [2]
Breccia complex	Magmatic breccia Río Blanco	Matrix biotite-1	$^{40}Ar/^{39}Ar$	5.06 ± 0.03 [3]	A. Skewes, unpub. report (1997) [2]
		Matrix biotite-2	$^{40}Ar/^{39}Ar$	4.85 ± 0.05 [3]	A. Skewes, unpub. report (1997) [2]
		Matrix K-feldspar	$^{40}Ar/^{39}Ar$	4.82 ± 0.05 [3]	A. Skewes, unpub. report (1997) [2]
	Granodiorite Río Blanco clasts in magmatic breccia	Biotite	$^{40}Ar/^{39}Ar$	4.81 ± 0.03 [3]	A. Skewes, unpub. report (1997) [2]
		K-feldspar	$^{40}Ar/^{39}Ar$	4.79 ± 0.03 [3]	A. Skewes, unpub. report (1997) [2]
	Magmatic breccia Río Blanco	Biotite	$^{40}Ar/^{39}Ar$	4.51 ± 0.05 [3]	A. Skewes, unpub. report (1997) [2]
		K-feldspar	$^{40}Ar/^{39}Ar$	4.34 ± 0.23 [3]	A. Skewes, unpub. report (1997) [2]
	Sur-Sur mineralized tourmaline breccia	Sericite whole rock	$^{40}Ar/^{39}Ar$	5.42 ± 0.09	Frikken et al. (2005)
		Biotite cement	$^{40}Ar/^{39}Ar$	4.78 ± 0.04	Frikken et al. (2005)
	Tourmaline breccia?,	Matrix Biotite	$^{40}Ar/^{39}Ar$	5.34 ± 0.02 [3]	A. Skewes, unpub. report (1997) [2]
	Río Blanco	Matrix K-feldspar	$^{40}Ar/^{39}Ar$	5.25 ± 0.07 [4]	A. Skewes, unpub. report (1997) [2]
	Molybdenite breccia	Molybdenite	Re/Os	5.31 ± 0.03	Mathur et al. (2001)
		Molybdenite	Re/Os	5.50 ± 0.03	Mathur et al. (2001)
		Molybdenite	Re/Os	6.26 ± 0.04	Mathur et al. (2001)
Late porphyries	Quartz monzonite porphyry	K-feldspar	Re/Os	5.20 ± 0.12 [4]	F. Munizaga, unpub. report (1994) [1]
		Whole rock	K-Ar	5.15 ± 0.2	Blondel (1980)
		K-feldspar	K-Ar	5.15 ± 0.32	Blondel (1980)
	Don Luis porphyry	K-feldspar	$^{40}Ar/^{39}Ar$	4.87 ± 0.37 [4]	F. Munizaga, unpub. report (1994) [1]
		Magmatic biotite	K-Ar	4.73 ± 0.16	Quirt et al. (1971), recalculated
		Whole rock	K-Ar	4.5 ± 0.4	Rojas (1985)
		Biotite	K-Ar	3.9 ± 0.7	Rojas (1985)
La Copa volcanic complex	Postore rhyolite	Magmatic biotite	K-Ar	4.03 ± 0.19	Quirt et al. (1971); recalculated
	Rhyolite tuff	Plagioclase	K-Ar	4.9 ± 0.2	Vergara and Drake (1978)
	Rhyolite tuff	Biotite	K-Ar	4.1 ± 0.1	Vergara and Drake (1978)
	Dacite porphyry dike	Biotite	K-Ar	4.9 ± 0.2 (1σ?)	Warnaars et al. (1985)
	Dacite porphyry	Biotite	K-Ar	4.8 ± 0.2 (1σ?)	Warnaars et al. (1985)

(PA) = plateau age comprising three heating steps and >50% ^{39}Ar released

[1] Documented in Serrano et al. (1996)

[2] Unpublished report for CODELCO, Andina Division

[3] Isochron age

[4] Weighted mean age

younger than many of the ages reported for the late porphyries. The precise age of mineralization, and its temporal relationships with the major late porphyry intrusions, therefore, remain poorly constrained. In particular, the available K-Ar–based data provide no firm evidence either that fertile hydrothermal activity persisted for a prolonged period or that this supergiant deposit was the product of multiple mineralizing events separated by significant hiatuses. The latter model is, however, favored by Mathur et al. (2001) on the basis of Re-Os ages for two molybdenites (Table 1).

The inferred magmatic and hydrothermal history of the Río Blanco-Los Bronces center is summarized in Table 2, largely after Serrano et al. (1996) but including the two recent $^{40}Ar/^{39}Ar$ ages reported by Frikken et al. (2005).

New Geochronologic Data

Sample locations and descriptions are documented in Table 3 and, in part, in three cross sections (Fig. 3), which further record the elevations of dated samples from contiguous transects.

The new geochronologic data are herein documented sample by sample, beginning with the U-Pb zircon analyses (Table 4; full data are recorded in Apps. 2 and 3), in sequence from the apparently oldest to the youngest. Incremental-heating Ar/Ar spectra for apparently magmatic biotite are then reported, in sequence from the oldest to the youngest of the host units, and the implications of these data are discussed in the context of the U-Pb data. Finally, we document the spot-fusion $^{40}Ar/^{39}Ar$ analyses of unequivocal hydrothermal minerals. Table 5 summarizes the Ar/Ar analytical data for incremental-heating and spot-fusion age determinations. All analytical procedures are described in Appendix 1; full $^{40}Ar/^{39}Ar$ data are given in Appendix 4.

ID-TIMS U-Pb zircon age data

Farellones Formation: Two samples of altered andesitic lavas were selected from drill core to establish the age span represented by the thick succession of subaerial volcanic flows and pyroclastic rocks, which was interpreted by Vergera et al. (1988) to be a roof pendant within the San Francisco batholith (Figs. 2, 3A). Of these, Andesite-1 was sampled from an elevation of 3,491 m a.s.l. and Andesite-2 from 3,235 m a.s.l. Both rocks give middle Miocene $^{206}Pb/^{238}U$ ages. Thus, in the $^{206}Pb/^{238}U$ versus $^{207}Pb/^{235}U$ concordia plot (Fig. 4A), the stratigraphically older andesite (-2) yielded four precise, concordant, overlapping analyses for large fractions of clear, inclusion-free and unfractured zircons, with a weighted mean age of 17.20 ± 0.05 Ma and an MSWD of 0.82 (Table 4). The seven unabraded small fractions separated from Andesite-1 included some cloudy and fractured crystals and, whereas five analyses fall on the concordia, two gave slightly and much older ages, indicative of the presence of inherited zircon (fractions B and G: Fig. 4B). Of the five concordant fractions, D, E, and F required acid flotation treatment to remove abundant pyrite and may, therefore, have suffered minor lead loss. We propose that the best age for crystallization of Andesite-1 is given by the total $^{206}Pb/^{238}U$ range for fractions A and C (i.e., 16.77 ± 0.25 Ma for step A). Regression through all of the data yields an upper intercept of 1.97 Ga, implying a Paleoproterozoic age for the inherited zircon component in fraction G.

San Francisco batholith: Three different samples from this granitoid complex were selected from underground exposures and drill core for U-Pb dating. These represent the areally extensive Río Blanco granodiorite and Cascada granodiorite, and the diorite, which forms restricted enclaves, dikelike bodies, and larger apophyses intruding the granodioritic rocks

TABLE 2. Inferred Magmatic-Hydrothermal History of the Río Blanco Porphyry Copper Deposit, Central Chile[1]

Rock unit/alteration	Inferred age range (Ma)
Farellones Formation	21–11
San Francisco batholith	20.1–7.4
Mineralized breccias	7.3–4.2
Potassic alteration	>5.4
Late porphyries	5.2–3.9

[1] After Serrano et al. (1996), including data from Frikken et al. (2005)

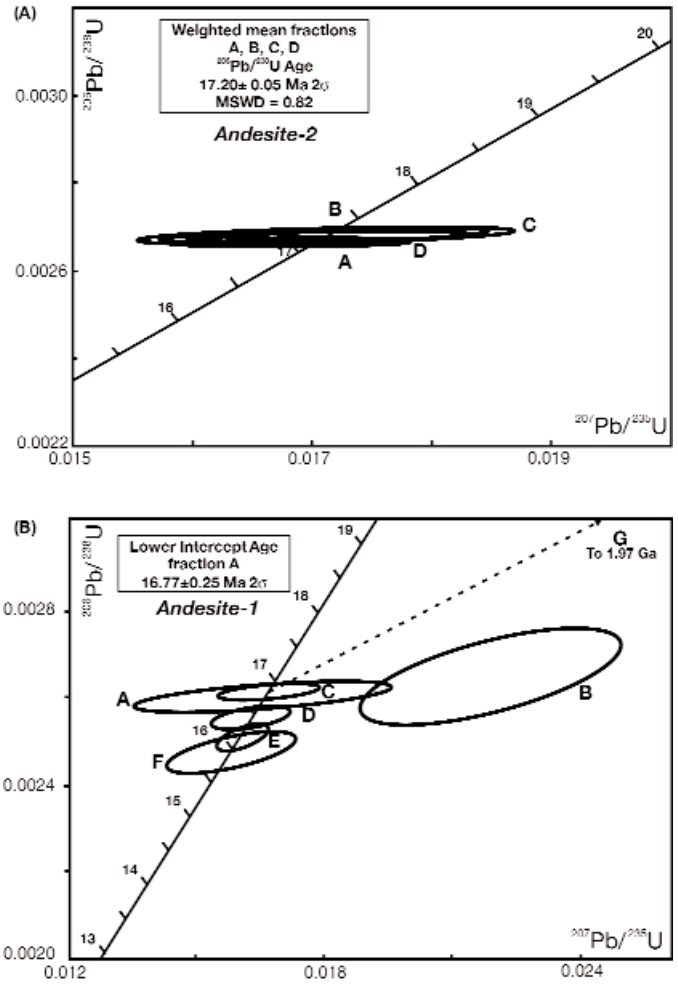

FIG. 4. $^{206}Pb/^{238}U$ vs. $^{207}Pb/^{235}U$ concordia plots for the Farellones Formation andesites. A. Andesite-2 from section 125 (4 zircon fractions), Río Blanco sector. B. Andesite-1 from section 275 (7 zircon fractions), Don Luis sector.

TABLE 3. Description of Dated Samples, Río Blanco Deposit

Rock unit	Sample	Dated mineral/vein	Method	Description	Alteration
GDRB-1	DDH173 – 223 m 2870 m a.s.l.; section 165	Biotite	$^{40}Ar/^{39}Ar$[1]	Magmatic biotite as xenocrysts and fine-grained hornblende replaced by secondary fine biotite; some biotite locally totally chloritized; calcite; small chlorite vein	Slight potassic alteration
GDRB-2	DDH173 – 30 m 3020 m a.s.l.; section 165	Biotite	$^{40}Ar/^{39}Ar$[1]	Magmatic biotite; hornblende locally with biotite replacement; chloritized hornblende; calcite	Slight potassic alteration
Diorite	DDH742 – 106.5 m 3184 m a.s.l.; section 305	Biotite	$^{40}Ar/^{39}Ar$[1]	Magmatic + hydrothermal biotite; magmatic biotite partly replaced by chlorite and secondary fine-grained biotite	Potassic alteration; anhydrite; chlorite
PQM-1	DDH577 – 28.7 m 3184 m a.s.l.; section 235	Biotite	$^{40}Ar/^{39}Ar$[1]	Magmatic biotite; some biotite xenocrysts partly replaced by secondary biotite/chlorite; calcite; anhydrite	Potassic with slight to stronger phyllic overprint
PQM-2	DDH231 – 155 m 3070 m a.s.l.; section 135	Biotite	$^{40}Ar/^{39}Ar$[1]	Magmatic biotite partly to totally chloritized; fresh magmatic biotite; ankerite in biotite; anhydrite; rare tourmaline in biotite; sericite + calcite replacing feldspar xenocrysts; quartz-feldspar matrix relatively unaltered; apatite in biotite	Potassic with slight phyllic overprint
PF	DDH738 – 276 m 3184 m a.s.l.; section 245	Biotite	$^{40}Ar/^{39}Ar$[1]	Magmatic biotite with chloritized and minor secondary biotite borders; sericite/muscovite; (potassic feldspar)-quartz-gypsum-anhydrite vein	Potassic with slight phyllic overprint (sericitization)
PDL stock	DDH746 – 302 m 3184 m a.s.l.; section 305	Biotite	$^{40}Ar/^{39}Ar$[1]	Magmatic + some hydrothermal biotite; anhydrite in matrix; some gypsum; some plagioclase grains are strongly sericitized	Slight potassic alteration
GDCC	DDH728 – 157.1 m 3070 m a.s.l.; section 345	Biotite vein	$^{40}Ar/^{39}Ar$[2]	Gypsum replacing fine-grained biotite vein; magmatic biotite; secondary biotite cluster; quartz-sericite-pyrite vein cuts biotite vein; anhydrite	Potassic with strong phyllic overprint
GDCC	DDH728 – 163.8 m 3070 m a.s.l.; section 345	Biotite vein	$^{40}Ar/^{39}A$[2]	Biotite vein cut by quartz-pyrite vein	Potassic with phyllic overprint
GDCC	DDH735 – 194.3 m 3286 m a.s.l.; section 325	K-feldspar vein	$^{40}Ar/^{39}Ar$[2]	Magmatic biotite totally replaced by fine-grained hydrothermal biotite; chlorite; gypsum and quartz-sericite vein	Potassic with strong phyllic overprint;
BXMGD	TSS22 – 802 m 2870 m a.s.l.; section 50	K-feldspar vein	$^{40}Ar/^{39}Ar$[2]	Partly chloritized biotite matrix; sericite/muscovite vein; potassic feldspar vein with partly sericite; calcite in biotite; anhydrite in sericite patches	Strong phyllic alteration
GDCC	DDH735 – 200 m 3286 m a.s.l.; section 325	Quartz-sericite vein	$^{40}Ar/^{39}Ar$[2]	Chloritized magmatic biotite replaced by secondary biotite agglomeration; quartz-sericite halo on gypsum-anhydrite-pyrite vein; sericite replacing primary biotite	Potassic with strong phyllic overprint
PDL	DDH746 – 37.5 m 3184 m a.s.l.; section 305	Quartz-sericite vein	$^{40}Ar/^{39}Ar$[2]	Magmatic biotite with calcite and sericite/muscovite replacement; quartz-sericite vein	Strong phyllic alteration
Andesita-1	PZ-2007 57-63 m 3491 m a.s.l. section 275	Zircon	$^{206}Pb/^{238}U$[3]	Chloritized biotite; sericitization of feldspar; two chloritized biotite veins cut each other;	Potassic alteration with slight phyllic overprint
Andesite-2	Segment CP-63 3235 m a.s.l.; section 125	Zircon	$^{206}Pb/^{238}U$[3]	Very fine grained chloritized biotite matrix; anhydrite vein with tourmaline needles; sericitization	Potassic alteration
GDRB	Segment GH-50 3224 m a.s.l.; section 155	Zircon	$^{206}Pb/^{238}U$[3]	Chloritized secondary biotite; anhydrite with tourmaline/actinolite needles; sericitization; quartz-sericite-anhydrite vein with some calcite cut by gypsum vein	Potassic with strong phyllic overprint
GDCC	DDH685 – 276-282 m 3184 m a.s.l.; section 375	Zircon	$^{206}Pb/^{238}U$[4]	Chloritized secondary biotite; anhydrite; sericitization; some calcite	Potassic with strong phyllic overprint
Diorite	DDH641 – 160-170 m 3184 m a.s.l.; section 295	Zircon	$^{206}Pb/^{238}U$[4]	Magmatic biotite replaced by secondary biotite or chlorite; anhydrite; quartz-gypsum-sericite-anhydrite vein	Potassic with phyllic overprint
PQM	Segment CP-63 3224 m a.s.l.; section 105	Zircon	$^{206}Pb/^{238}U$[3]	Magmatic biotite replaced by secondary biotite or chlorite; sericitization of potassic feldspar phenocrysts not affecting the matrix	Potassic alteration
PF	DDH742 – 7-13 m 3184 m a.s.l.; Setion 305	Zircon	$^{206}Pb/^{238}U$[3]	Magmatic + secondary biotite; sericitization of feldspar/plagioclase; anhydrite, calcite; quartz-potassic feldspAr/anhydrite vein	Strong phyllic alteration
PDL	Loop Chancador Don Luis 3132 m a.s.l.; section 265	Zircon	$^{206}Pb/^{238}U$[3]	Magmatic + secondary biotite with calcite; fine quartz-vein; some anhydrite replacing potassic feldspar	Slight potassic alteration

Abbreviations: BXMGD = Magmatic breccia in Cascada granodiorite, GDCC = Cascada granodiorite, GDRB = Río Blanco granodiorite, PDL = Don Luis porphyry, PF = Feldspar porphyry, PQM = Quartz monzonite porphyry

[1] Step heating

[2] Spot fusion

[3] U/Pb on zircon fractions

[4] U/Pb on zircon single grains

TABLE 4. $^{206}Pb/^{238}U$ Zircon Age Data by Isotope Dilution Thermal Ion Mass Spectrometry and, in the Dacite Plug, Sensitive High Resolution Ion Microprobe

Sample	Location	$^{206}Pb/^{238}U$ (Ma) (±2σ)	MSWD
Andesite-1	PZ-2007 (57-63 m), nivel 11 Section 275	16.77 ± 0.25	-
Andesite-2	Segment CP-63, nivel 16 Section 125	17.20 ± 0.05	0.82
Río Blanco granodiorite	Segment GH-50, nivel 16-½ Section 155	11.96 ± 0.40	-
Diorite	DDH641 (160-170 m), nivel 17 Section 295	8.19 ± 0.46[1] 8.84 ± 0.05	0.78 10.8
Cascada granodiorite	DDH685 (276-282 m), nivel 17 Section 375	8.4 ± 0.23[2]	-
Quartz monzonite porphyry	Segment CP-63, nivel 16-½ Section 105	6.32 ± 0.09	-
Feldspar porphyry	DDH742 (7-13 m), nivel 17 Section 305	5.84 ± 0.03	-
Don Luis porphyry	Loop Chancador Don Luis; nivel 18 Section 265	5.23 ± 0.07	-
Dacite plug	XC-155; nivel 16-½ Section 155	4.92 ± 0.09	1.3

[1] Weighted mean of two individual grains
[2] One individual grain

TABLE 5. $^{40}Ar/^{39}Ar$ Geochronological Results

Sample	Drill core	Grain size (μm)	TGA[1] (Ma) (±2σ)	PA[2] (Ma) (±2σ)	IIA[3] (Ma) (±2σ)	MSWD
Biotite step heating:						
Río Blanco granodiorite-1	DDH173 (223 m) Section 165	250–500	11.19 ± 0.42	10.98 ± 0.33	10.95 ± 0.41	0.05
Río Blanco granodiorite-2	DDH173 (30 m) Section 165	425–500	11.62 ± 0.07	11.59 ± 0.08	11.57 ± 0.14	2.25
Diorite	DDH742 (106.5 m) Section 305	250–300	4.63 ± 0.20	4.60 ± 0.13	4.51 ± 0.23	0.63
Quartz monzonite porphyry-1	DDH577 (28.7 m) Section 235	500–1000	4.82 ± 0.11	4.75 ± 0.10	4.71 ± 0.11	0.94
Quartz monzonite porphyry-2	DDH231 (155 m) Section 135	180–250	5.15 ± 0.08	5.12 ± 0.07	5.08 ± 0.08	1.35
Feldspar porphyry	DDH738 (276 m) Section 245	500–1000	4.64 ± 0.08	4.62 ± 0.08	4.61 ± 0.09	0.17
Don Luis porphyry stock	DDH746 (302 m) Section 305	150–180	4.60 ± 0.06	4.57 ± 0.06	4.54 ± 0.11	1.29

Sample	Drill core	Vein	No. spots	Weighted mean age (Ma) (± 2σ)	MSWD
Spot-fusion results:					
Cascada granodiorte	DDH728 (157.1 m) Section 345	Biotite	4	5.32 ± 0.27	1.17
Cascada granodiorte	DDH728 (163.8 m) Section 345	Biotite	6	4.59 ± 0.11	0.66
Cascada granodiorte	DDH735 (194.3 m) Section 325	Potassic feldspar	5	5.25 ± 0.13	0.56
Magmatic breccia	TSS-22 (802 m) Section 50ss	Potassic feldspar	5	4.67 ± 0.12	1.51
Cascada granodiorte	DDH735 (200 m) Section 325	Sericite (muscovite)	5	4.40 ± 0.15	0.78
Don Luis porphyry	DDH746 (37.5 m) Section 305	Sericite (muscovite)	5	4.37 ± 0.06	1.74

[1] Total gas age
[2] Plateau age
[3] Inverse isochron age

in the Sur-Sur sector (Fig. 3A-C). The Río Blanco granodiorite is combined with the Cascada granodiorite in Figure 2.

Six unabraded zircon fractions of varied morphology were analyzed (Fig. 5A; Table 4) from the Río Blanco granodiorite sample, taken from "tramo" GH-50 of the Río Blanco underground mine. Fractions A and B were of elongated prisms and yielded ages of ca. 13 Ma, whereas the stubby prismatic grain fractions, C through F, cluster around the concordia at ca. 12 Ma (Fig. 5A). The former two fractions are interpreted as containing inherited zircon domains, and the preferred intrusion age of this unit is 11.96 ± 0.40 Ma, the overall range of $^{206}Pb/^{238}U$ ages for fractions C through F.

The Cascada granodiorite was sampled from drill core 685 (276–282 m intercept), at a mean elevation of 3,184 m a.s.l. Three abraded single zircon grains (e.g., Fig. 6A) yielded ages plotting in concordia at ca. 10.4 Ma (Z1), 8.4 Ma (Z2) and 9.1 Ma (Z3; Fig. 5B). Of these zircons, Z1 and Z3 are interpreted as containing inherited components, and the age of crystallization is taken to be 8.4 ± 0.23 Ma. The diorite, taken from drill core at 3,184 m a.s.l., was dated both conventionally using unabraded grain fractions (Fig. 5C) and with abraded single grains (Fig. 5D). Five of six fractions of different morphologies (A, C, D, E, and F) yielded concordant results with a weighted mean $^{206}Pb/^{238}U$ age of 8.84 ± 0.05 Ma and an MSWD of 10.8. Fraction B, however, gave a significantly older age of 12.6 Ma (Fig. 5C), interpreted as evidence of an inherited component. Of the four single grains (Fig. 6B: Z1-Z4), two (Z3, Z4) yielded ages of 8.0 and 8.4 Ma (Fig. 5D), essentially identical to those given by the majority of the zircon fractions, whereas grains Z2 and Z1 yielded, respectively, moderately and markedly older ages of 11.1 and 17.2 Ma. Our best estimate of the age of the diorite is the weighted mean, 8.16 ± 0.45 Ma (MSWD = 0.78) for single grains Z3 and Z4.

Late porphyries: Zircons have been dated from the three petrographically distinct units recognized by mine personnel as constituting the late porphyry intrusion complex (Fig. 2: quartz monzonite porphyry, feldspar porphyry, and Don Luis porphyry).

Seven unabraded zircon fractions (A-G), each comprising clear, colorless to pale pink, coarse, stubby to elongate-prismatic, euhedral with multifaceted terminations, were dated from a quartz monzonite porphyry sample collected from the 16-1/2 level (3,210 m a.s.l.) of the Río Blanco mine. Six fractions yielded concordant but not overlapping ages (Fig. 7A), among which B, D, and F exhibit a minor inherited component. Fractions C and E, in contrast, clearly incorporate considerable inherited Pb. Two calculated linear regression lines reveal upper intercept ages of 414 Ma and 1.52 Ga,

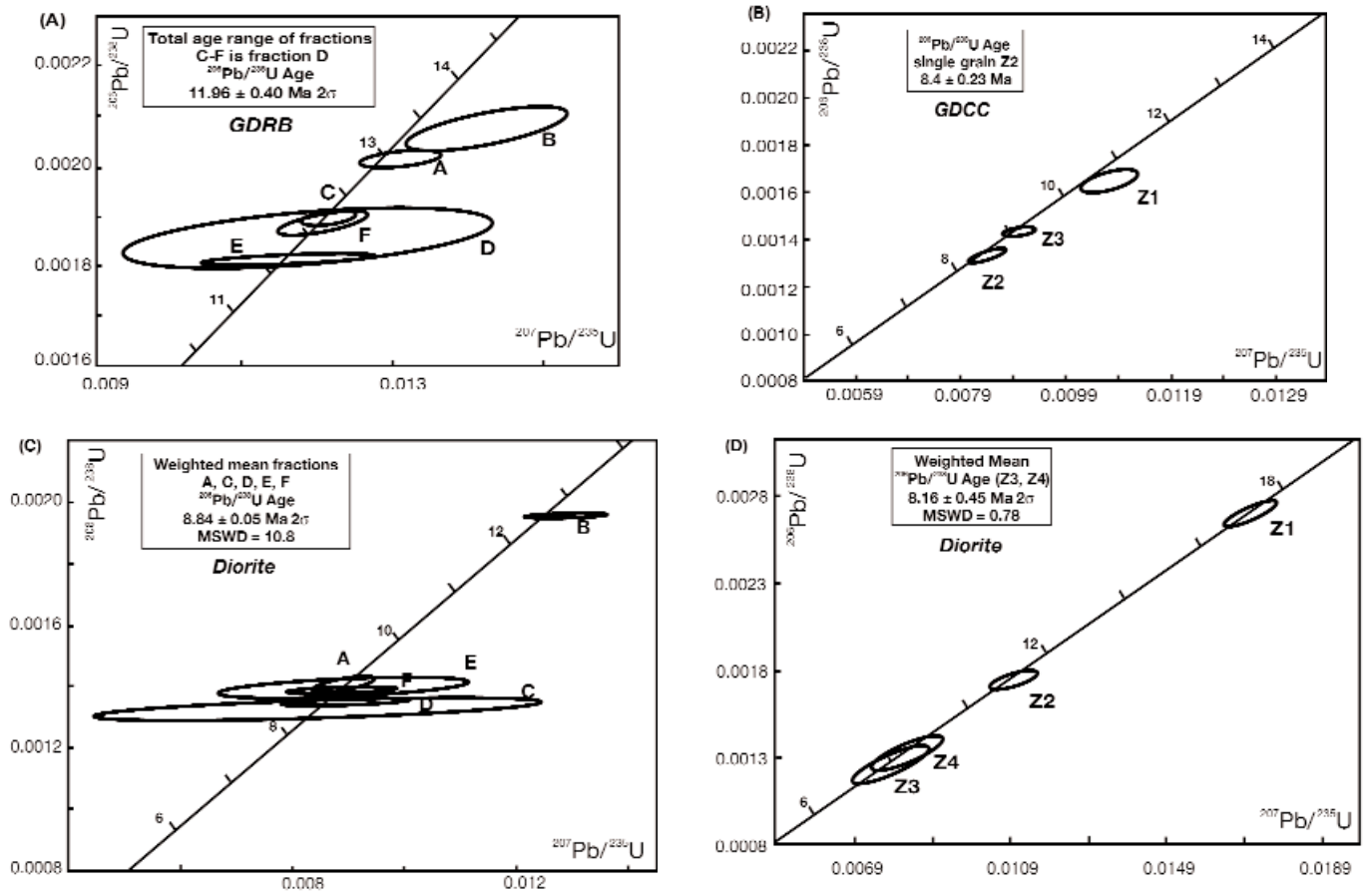

FIG. 5. $^{206}Pb/^{238}U$ vs. $^{207}Pb/^{235}U$ concordia plots for units of the San Francisco batholith.. A. Río Blanco granodiorite from section 155 (6 zircon fractions), Río Blanco sector. B. Cascada granodiorite from section 375 (3 single grains), Don Luis sector. C. Diorite from section 295 (6 zircon fractions), Don Luis sector. D. Diorite from section 295 (4 single grains), Don Luis sector. Abbreviations: GDCC = Cascada granodiorite, GDRB = Río Blanco granodiorite.

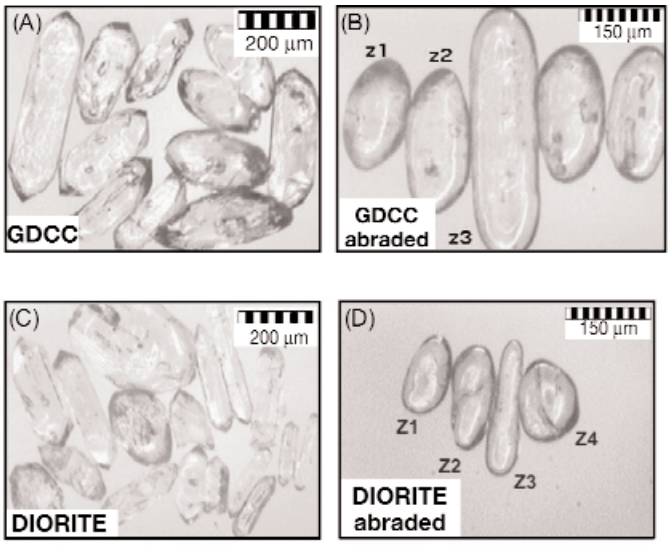

FIG. 6. Photomicrographs of single zircon grains used for ID-TIMS analyses. Cascada granodiorite: (A) natural and (B) abraded zircons. Diorite: (C) natural and (D) abraded zircons.

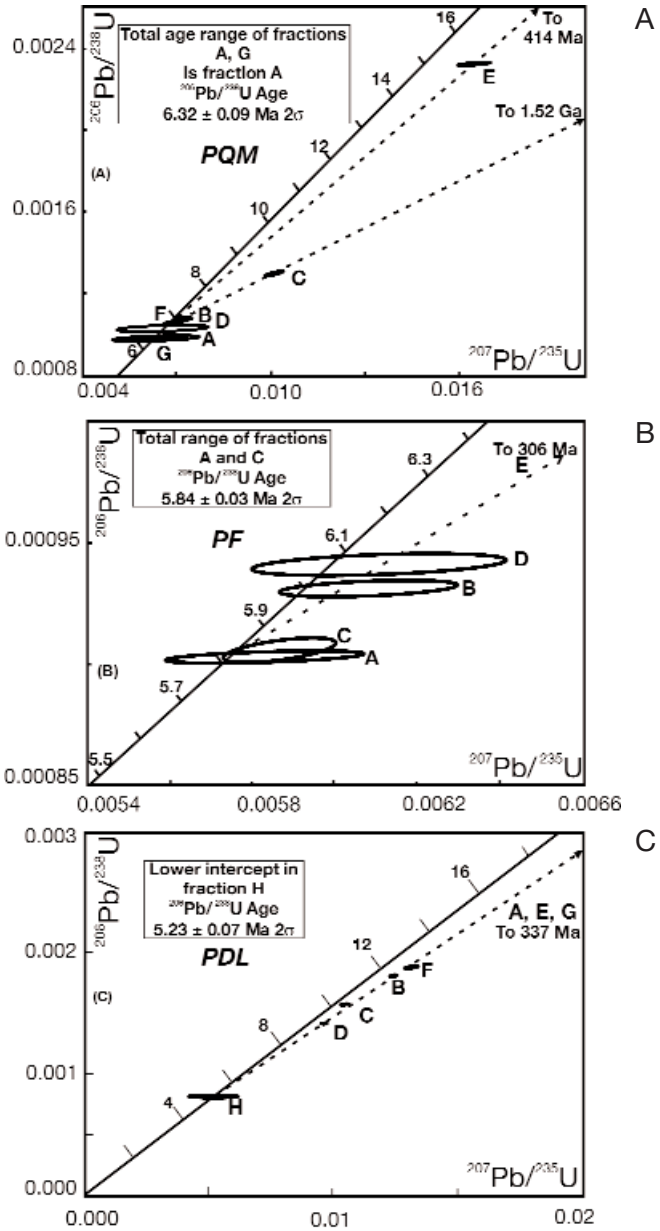

FIG. 7. $^{206}Pb/^{238}U$ vs. $^{207}Pb/^{235}U$ concordia plots for late porphyries. A. Quartz monzonite porphyry from section 105 (7 zircon fractions), Río Blanco sector. B. Feldspar porphyry from section 305 (5 zircon fractions), Don Luis sector. C. Don Luis porphyry from section 265 (8 zircon fractions), Don Luis sector.

respectively, Devonian and Mesoproterozoic, supporting the records of xenocrystic basement zircons in Andean igneous rocks in central Chile (Zentilli et al., 2001). Whereas Proterozoic basement rocks are exposed only in the Sierra Pampeanas, central-west Argentina (e.g., Kay et al., 1996), Paleozoic rocks crop out in the eastern parts of the central Andean Cordillera, as well as in the Coastal Cordillera of central Chile (Vergara and Drake, 1979). The best estimate of the time of emplacement of quartz monzonite porphyry is given by the total age range given by fractions A and G, which overlap but are best represented by step A, yielding an age of 6.32 ± 0.09 Ma with an MSWD of 0.12.

Five unabraded zircon fractions of feldspar porphyry were extracted from a 6-m length of DDH 742 at a mean elevation of 3,184 m a.s.l. One of these (E), comprising elongated prismatic grains, yielded (Fig. 7B) an older apparent age than did fractions A through D, which were dominated by stubby, prismatic grains. The latter, moreover, although plotting on the concordia, embrace a significant range of apparent ages. Fractions A and C overlap, but the best age and, hence, time of intrusion of this body is represented by step C (5.84 ± 0.03 Ma).

Four fractions (A-D) of large, stubby, prismatic grains were separated from a Don Luis porphyry sample taken from the Loop Chancador on level 18 of the Río Blanco mine at an elevation of 3,132 m a.s.l. These were abraded prior to dissolution to minimize the effects of postcrystallization Pb loss. This was apparently minimal, and the other fractions were therefore not abraded. In addition, four fractions (E-G) of coarse, pale pink, multifaceted and elongate-prismatic grains were analyzed. All fractions, irrespective of morphology, incorporate inherited material and define a linear regression (Fig. 7C) with intercepts of 5.23 ± 0.07 and 337 Ma. The younger intercept (unabraded fraction H) is accepted as a precise age for Don Luis porphyry.

SHRIMP ^{238}U-^{206}Pb zircon age data

Twenty-two analyses were carried out on 18 zircon grains selected from dacitic (i.e., igneous) material from the strongly brecciated and intensely sericitized western margin of the dacite plug unit (Fig. 3A). Cores and rims were analyzed in grains with more complex internal structures, visible in cathodoluminescence images (Fig. 8). The central areas of grains 13 and 16 yielded ages of 40.9 and 174.3 Ma, respectively, clearly recording inherited material. Because of very low U and Th contents, the data obtained for the core of grain 5 were similarly omitted from the age calculation. The remaining ages range between 4.55 and 5.88 Ma. In the summed Gaussian probability plot of 19 sets of data (Fig. 9) the calculated weighted mean age is 4.96 ± 0.12 Ma (95% confidence) with an MSWD of 2.3 and low probability of

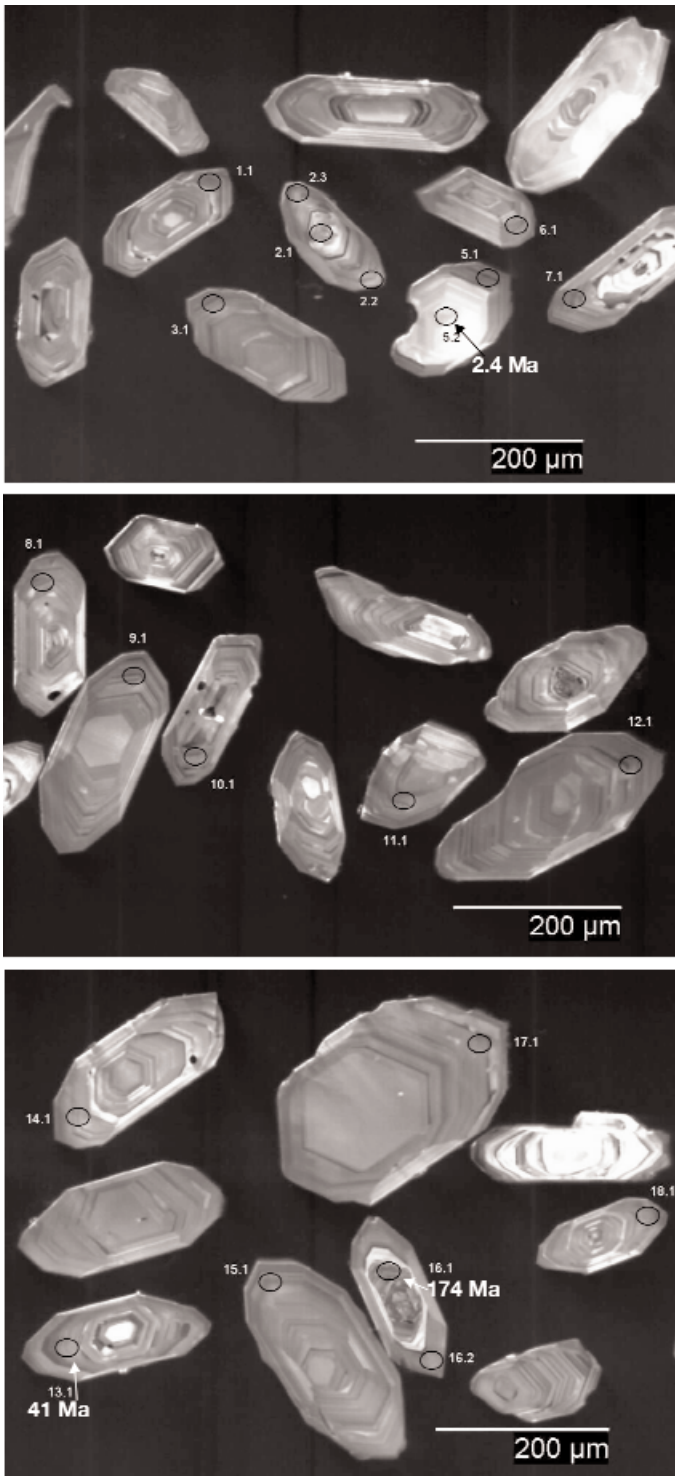

FIG. 8. Cathodoluminescence images of zircon grains from sample of dacite plug used for U/Pb SHRIMP II analyses. Numbers indicate grain spots (App. 3). Analyzed areas are outlined.

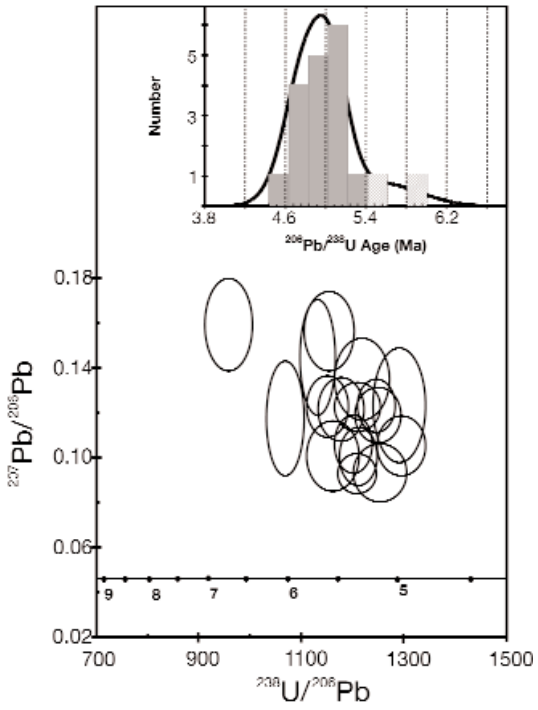

FIG. 9. $^{207}Pb/^{206}Pb$ vs. $^{238}U/^{206}Pb$ Tera-Wasserburg concordia with cumulative Gaussian plot for 18 single-grain zircon analyses for dacite plug, Río Blanco sector.

0.001. Excluding the two oldest ages of 5.88 and 5.58 Ma (weighted mean of 5.69 ± 0.32 Ma), the new calculated weighted mean age accommodating 17 analyses is 4.92 ± 0.09 Ma (95% confidence) with a probability of 0.21 and an MSWD of 1.3. The latter age, excluding inherited components of ca. 174, ca. 41, and 5.69 ± 0.32 Ma in age, is interpreted as the crystallization age of the dacite plug.

$^{40}Ar/^{39}Ar$ incremental-heating biotite ages

Whereas the U-Pb data were presented in sequence of decreasing zircon age, the $^{40}Ar/^{39}Ar$ step-heating data are discussed in the order of decreasing age of the host intrusion as given by the zircon ages. In general, total gas ages, plateau ages, and inverse isochron ages are concordant within 2σ error, excluding major problems caused by either excess argon or partial argon loss. Salient analytical data are reported in Table 5 and in the age spectra of Figures 10, 13, and 15; full data are given in Appendix 4.

San Francisco batholith: Age spectra were obtained by laser-induced step heating of biotite separates from the Río Blanco granodiorite and diorite units of the San Francisco batholith. The analyzed samples of biotite occurred as dispersed, coarse flakes with euhedral to subhedral forms, were not associated with crosscutting veinlets and are interpreted as magmatic rather than hydrothermal. They appear unaltered at the binocular microscope scale.

Two separates of biotite were analyzed from the Río Blanco granodiorite. Biotite (250–500 μm fraction), from sample GDRB-1 yielded a total gas age of 11.19 ± 0.42 Ma from nine heating increments (Fig. 10A). The plateau age, representing 98 percent of ^{39}Ar released, is 10.98 ± 0.33 Ma, with an MSWD of 0.05. The inverse isochron age (Table 5) is concordant with the plateau age. A 425- to 500-μm concentrate from a second sample, GDRB-2 (DDH 173, 30 m intercept), yielded a seven-step age plateau at 11.59 ± 0.08 Ma (Fig. 10B) accommodating 99.9 percent of the ^{39}Ar released. The

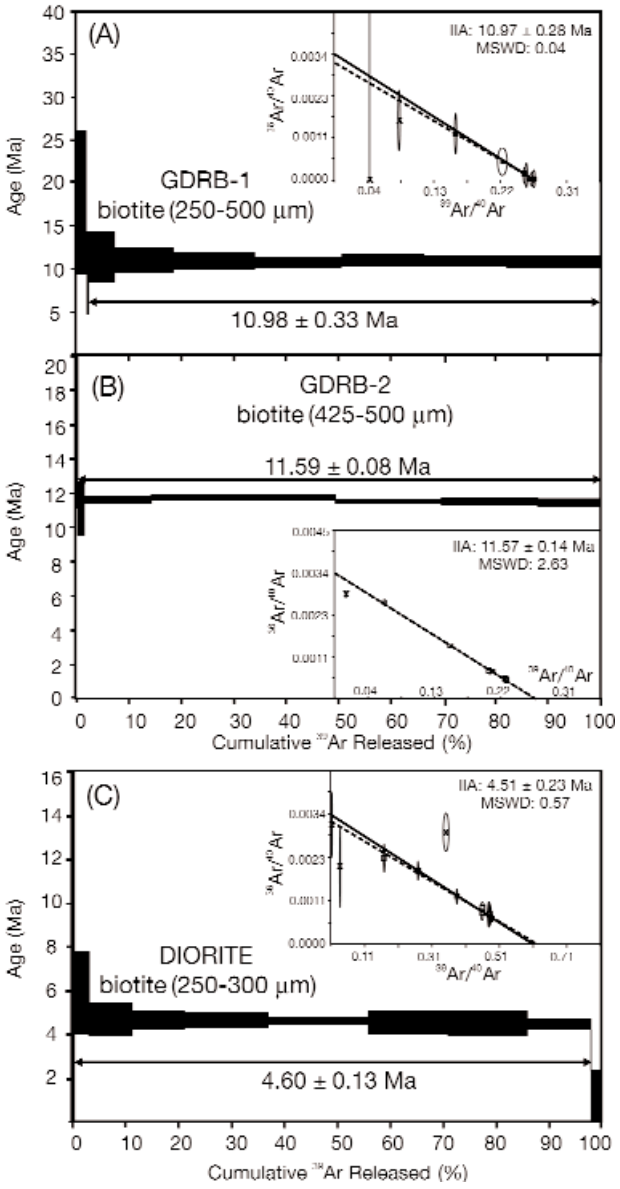

FIG. 10. $^{40}Ar/^{39}Ar$ biotite age spectra and inverse isochron plots for San Francisco batholith. A. Río Blanco granodiorite (GDRB-2) from section 165, Río Blanco sector. B. Río Blanco granodiorite (GDRB-1) from section 165, Río Blanco sector. C. Diorite from section 305, Don Luis sector.

MSWD for the plateau age is relatively high, at 2.25. The first three steps, at 700º to 1,000ºC, have increasing apparent ages, whereas the apparent ages of the high-temperature steps decrease successively until fusion of the sample at 1,400ºC. The inverse isochron age, 11.57 ± 0.14 Ma, is interpreted as an errorchron but is within error of the plateau age.

Despite the higher errors in the plateau age for GDRB-1, the absence of a progressive decrease in apparent age with increasing laser temperature suggests that it may be a more reliable record of the time of postmagmatic Ar retention in the biotite of this unit of the batholith than the significantly older date determined for GDRB-2 biotite. The age spectrum for that sample (Fig. 10B) exhibits a configuration suggestive of reactor-induced ^{39}Ar recoil, a common problem with chloritized biotite. In such cases, the highest temperature step, here 11.43 ± 0.19 Ma, within 2σ error of the plateau age of GDRB-1, may approach the true age. Both, however, are in permissive agreement with our preferred U-Pb age, 11.96 ± 0.40 Ma, for intrusion of the Río Blanco granodiorite and may record different stages in its cooling history.

Biotite (250–300 μm) in the diorite (DDH 742, 106.5 m) yielded an eleven-step age spectrum with a total gas age of 4.63 ± 0.20 Ma (Fig. 10C). Excluding the first two aberrant steps and the last step, a plateau age of 4.60 ± 0.13 Ma was calculated from eight consecutive steps representing 97.6 percent of the ^{39}Ar released and with an acceptable MSWD of 0.63. The biotite Ar/Ar age is ca. 3.5 m.y. younger than the zircon age for the diorite and must, therefore, record either quantitative outgassing and resetting of magmatic biotite during a later thermal event or the crystallization of hydrothermal biotite.

Late porphyries: The analyzed late porphyry biotites occur as dispersed euhedral to subhedral flakes unassociated with either veins or unambiguous pervasive K silicate or hydrolytic alteration and are, therefore, interpreted as phenocrystic (e.g., Fig. 11). Most are fresh, but restricted alteration to ankerite and minor chlorite is evident (Fig. 12). Moreover, the biotite grains separated from feldspar porphyry exhibit variable marginal development of fine-grained, clearly secondary biotite (Fig. 12A-B).

Coarse-grained, 0.5- to 1-mm, biotite flakes from the oldest of the late intrusions, the 6.32 ± 0.09 Ma quartz monzonite porphyry, yielded a slightly disturbed spectrum (Fig. 13A) with a total gas age of 4.82 ± 0.11 Ma and an eight-step plateau age of 4.75 ± 0.10 Ma (98% of ^{39}Ar released; MSWD = 0.94). The inverse isochron age of 4.71 ± 0.11 Ma is essentially concordant. Overall, the plateau exhibits progressively decreasing ages from 5.06 to 4.60 Ma, possibly evidence for ^{39}Ar recoil, and the age of the final increment may be the best record of the time of Ar retention. This age is ca. 1.6 m.y. younger than the zircon age for this unit, delimiting a probably unacceptably protracted interval for the monotonic cooling and crystallization of even a large hypabyssal body. A second biotite sample from this porphyry unit (PQM-2; 180–250 μm) yielded an undisturbed total gas age of 5.15 ± 0.08 Ma, a 100 percent plateau age of 5.12 ± 0.07 Ma

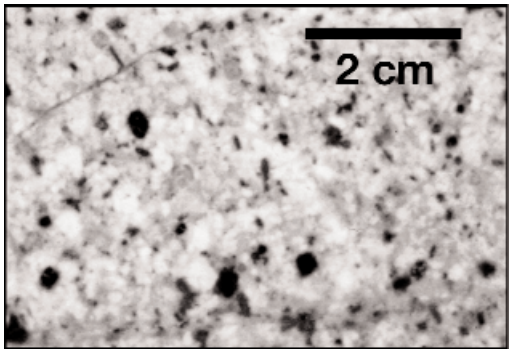

FIG. 11. Characteristic texture of quartz monzonite porphyry (PQM; DDH577; 28.7 m), showing apparently phenocrystic biotite "books" unassociated with veinlets or alteration.

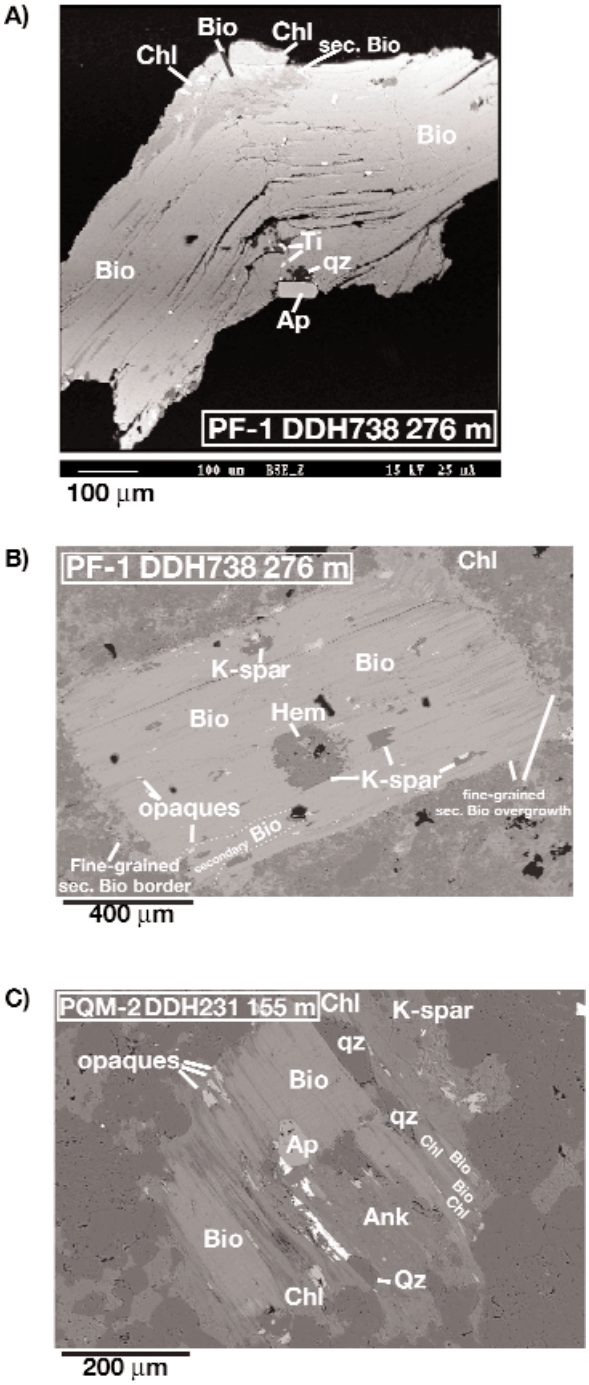

FIG. 12. Backscattered electron images of feldspar porphyry biotite. Feldspar porphyry single biotite grain from separate, showing development of secondary biotite, chlorite, and titanite (qz = quartz, Ap = apatite), and kinking probably resulting from specimen preparation. Feldspar porphyry biotite in thin section, showing extensive development of secondary biotite at grain boundaries and along cleavage planes (minerals as in Fig. 12A; Hem = hematite). PQM-2 biotite in thin section, showing chloritization along cleavage planes and patch of secondary ankerite (Ank).

(MSWD = 1.35), and a slightly younger inverse isochron age of 5.08 ± 0.08 Ma (Table 5, Fig. 13B).

Coarse biotite flakes (0.5–1 mm) from the 5.84 ± 0.03 Ma feldspar porphyry gave a total gas age of 4.61 ± 0.08 Ma (11 steps) and a plateau age of 4.62 ± 0.08 Ma from eight concordant steps and with a MSWD of 0.17 (Table 5, Fig. 13C).

Fine-grained, 150- to 180-μm, biotite from the youngest of the late intrusions, the 5.23 ± 0.07 Ma Don Luis porphyry, yielded a total gas age of 4.60 ± 0.06 Ma and an eleven-step plateau age of 4.57 ± 0.06 Ma (99.8% of ^{39}Ar released; MSWD = 1.29; Fig. 13D). The inverse isochron age, 4.54 ± 0.11 Ma with an ^{40}Ar/^{36}Ar ratio of 296.8, is within error of the total gas and plateau age.

^{40}Ar/^{39}Ar spot-fusion analyses

Six hydrothermal vein assemblages were dated (data summarized in Table 5) using the spot-fusion technique, in which from five to eight microscopic areas of each vein were fused by the laser beam, yielding a total gas age. The textural relationships of two dated assemblages hosted by Cascada granodiorite in the Don Luis sector are illustrated in Figure 14. Inverse isochron plots for each group of spot-fusion analyses are shown in Figure 15. In each case, analyses which are significantly older than the U-Pb crystallization age of the host-rock unit were rejected from the age calculation. In only one case, a biotite vein hosted by the Cascada granodiorite (DDH728: 163.8 m; Don Luis sector), were two age groups, at 7.01 and 5.32 Ma, distinguished. Of these, the preferred age is the younger because of its lower error and because the local chloritization of the mica may have caused ^{39}Ar recoil.

Four samples representative of K silicate alteration hosted by the 8.4 ± 0.23 Ma Cascada granodiorite in the Don Luis sector were examined. Four of eight spots in a veinlet of fine-grained (<200 μm) biotite yielded apparent ages ranging from 5.65 to 5.16 Ma, with an MSWD of 1.17 (Fig. 15A). The weighted mean age is 5.32 ± 0.27 Ma. The ^{40}Ar/^{36}Ar ratio of the four spots is 294.7, excluding the involvement of excess ^{40}Ar. Six of seven spots in a second fine biotite veinlet gave a markedly younger age, 4.59 ± 0.11 Ma, with an MSWD of 0.66 and a ^{40}Ar/^{36}Ar ratio of 299.2 (Fig. 15B). A K-feldspar vein yielded a weighted mean age of 5.25 ± 0.13 Ma from five of six spots, with an MSWD of 0.56 and a ^{40}Ar/^{36}Ar ratio of 303.9 (Fig. 15C).

The fourth sample representative of potassic alteration is from an orthoclase vein cutting both clasts and biotite-dominated matrix in a body of magmatic breccia, also hosted by the Cascada granodiorite but in the Sur-Sur sector. The weighted mean age of five or six spots is 4.67 ± 0.12 Ma, the individual ages ranging from 4.51 to 4.77 Ma, with an MSWD of 1.51 and a ^{40}Ar/^{36}Ar ratio of 307.9, slightly higher than the atmospheric value (Fig. 15D).

Finally, two sericite samples (two-layered monoclinic polytype muscovite, $2M_1$) were dated from quartz-sericite veins. One, from a 1-cm-wide, pyrite-bearing vein hosted by the Cascada granodiorite of the Don Luis sector, yielded a weighted mean age of 4.40 ± 0.15 Ma (five spots). Ages range from 4.85 to 4.27 Ma, with an MSWD of 0.78 and a ^{40}Ar/^{36}Ar ratio of 299.7, close to the atmospheric value (Fig. 15E). A second vein containing chalcopyrite and hosted by Don Luis porphyry (Don Luis sector) gave a very similar age of 4.37 ± 0.06 Ma; five of seven spots ranged from 4.23 to 4.42 Ma, with an MSWD of 1.74 and a ^{40}Ar/^{36}Ar ratio of 263.8 (Fig. 15F).

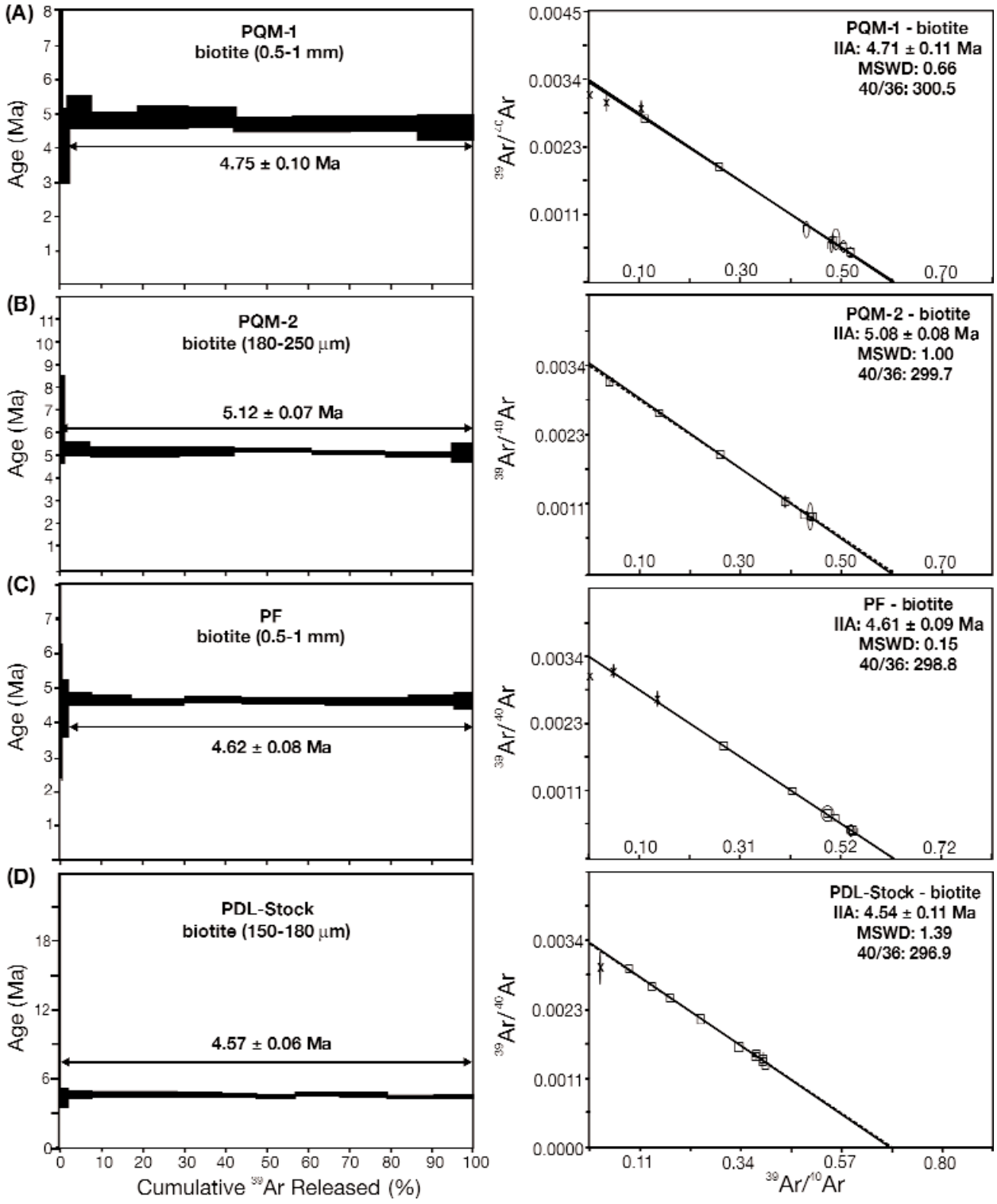

FIG. 13. $^{40}Ar/^{39}Ar$ biotite age spectra, indicating age plateaus and inverse isochron plots for late porphyries. Quartz monzonite porphyry-1, section 235, Don Luis sector. Quartz monzonite porphyry-2, section 135, Río Blanco sector. Feldspar porphyry, section 245, Don Luis sector. Don Luis porphyry stock, section 305, Don Luis sector.

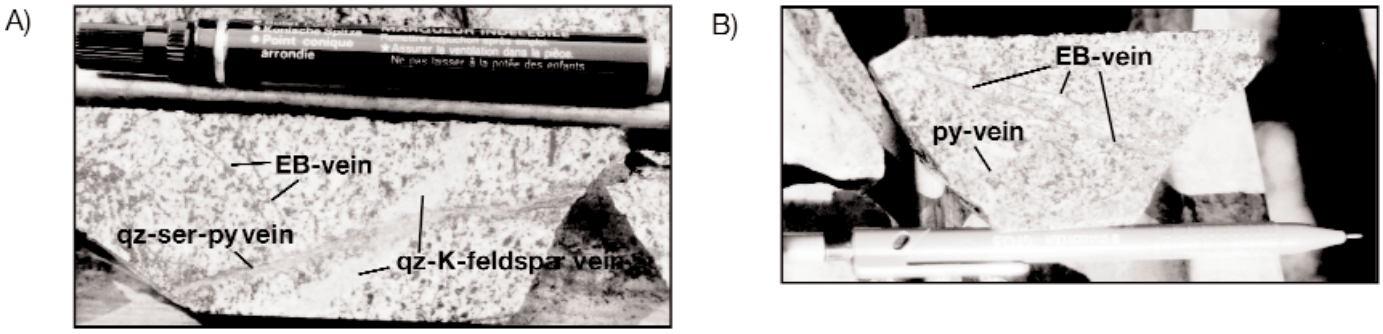

FIG. 14. Cascada granodiorite (DDH735; 194.3 m, Don Luis sector). A. Chloritized biotite and quartz-K-feldspar veins cut by quartz-sericite-pyrite vein. The quartz-feldspar vein itself cuts a chloritized biotite vein. The sample is characterized by pervasive potassic alteration with a strong phyllic overprint. qz = quartz; py = pyrite; ser = sericite; EB = early biotite. B. Cascada granodiorite (DDH728; 163.8 m, Don Luis sector). Biotite veins cut by pyrite veins. As in (A), pervasive K silicate alteration is overprinted by quartz-sericite-pyrite assemblages.

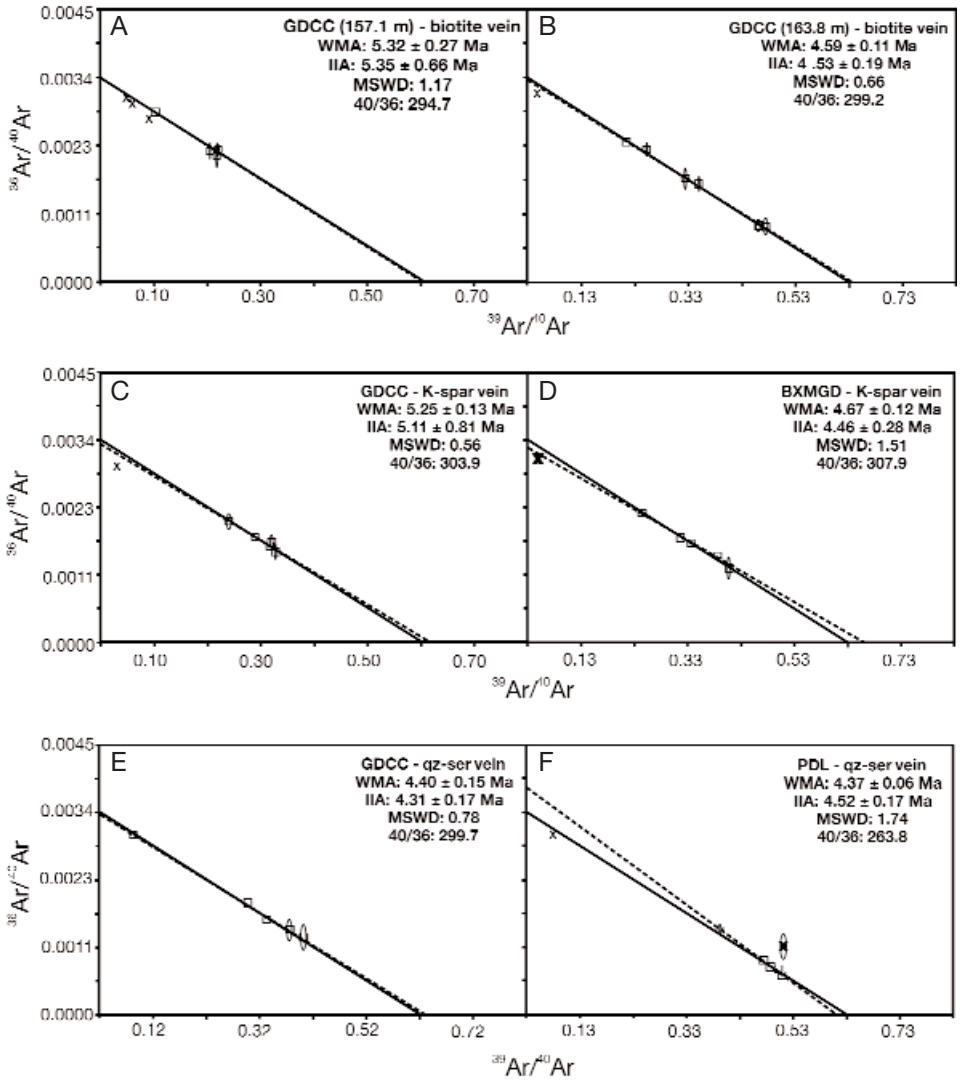

FIG. 15. Inverse isochron plots for spot-fusion $^{40}Ar/^{39}Ar$ analyses of vein assemblages. IIA = inverse isochron age, WMA = weighted mean age. A. Cascada granodiorite-hosted biotite vein, section 345, Don Luis sector. B. Cascada granodiorite-hosted biotite vein, section 345, Don Luis sector. C. Cascada granodiorite-hosted K-feldspar vein, section 325, Don Luis sector. D. Magmatic breccia of the Cascada granodiorite-hosted K-feldspar vein, section 50, Sur-Sur sector. E. Cascada granodiorite-hosted quartz-sericite vein, section 325, Don Luis sector. F. Don Luis porphyry quartz-sericite vein, section 305, Don Luis sector.

The two sericite spot-fusion ages are younger than those for biotite and K-feldspar, consistent with local geologic relationships, whereas the data overall define an interval of 5.32 to 4.37 Ma, similar to that exhibited by the apparently magmatic biotite in the late porphyries and the diorite (i.e., 5.12–4.57 Ma). Therefore, none of the spot-fusion ages disagree with the age relationships yielded by the other analytical methods.

Synthesis of Geochronologic Data

In a broader context, this research was designed to test the hypothesis that exceptionally large, high-grade porphyry systems are products of protracted and/or multiple magmatic-hydrothermal histories. In this section, we first synthesize the U-Pb zircon evidence for the succession of magmatic events which provide the setting for hydrothermal activity, thereafter addressing the more problematic $^{40}Ar/^{39}Ar$ database.

U-Pb chronology

Andesitic flows: The U-Pb ages for the two andesitic units confirm that the volcanic succession represents the Farellones, rather than the Abanico Formation, in conformity with the conclusions of Vergera et al. (1988, p. 207), who proposed that "the age of the largest volume of [Farellones Formation] extrusive rocks ranges from 18 to 15 Ma [the age interval of four of five K-Ar plagioclase ages], thus defining a major intensity of volcanism during the early and middle Miocene." We emphasize, however, that the new ages do not delimit the complete volcanic succession in the Río Blanco mine area.

Premineralization intrusive units: Our new zircon age data do not unambiguously define the absolute age relationships between the San Francisco batholith and the volcanic succession. Whereas three units of the batholith (viz. the Río Blanco granodiorite, the Cascada granodiorite, and the diorite) are shown to have been emplaced over a period of ca. 3.5 m.y. in the later middle Miocene (8.16 ± 0.45–11.96 ± 0.40 Ma), the significance of the older K-Ar mineral ages (13.6–20.1 Ma) reported for intrusive bodies by Warnaars et al. (1985) is unresolved. The 14.82 ± 0.12 Ma $^{40}Ar/^{39}Ar$ age reported by Serrano et al. (1996) for biotite from a quartz monzonitic unit may be evidence for initial development of the batholith prior to 12 Ma, but the sample site is 9 km south of the deposit and the age spectrum is disturbed. The Ar/Ar age may therefore represent only a maximum age for this intrusive unit. Warnaars et al. (1985) obtained a K-Ar age of 11.3 ± 0.4 Ma for this sample, in agreement with the Ar/Ar biotite and U-Pb zircon ages presented herein. However, some of the oldest hornblende K-Ar ages reported by Warnaars et al. (1985) for a hornblende diorite unit in the Los Bronces mine appear to disagree with our zircon ages for the prebatholith volcanism. The two younger U-Pb ages for the Cascada granodiorite (8.4 ± 0.23 Ma) and the diorite (8.16 ± 0.45 Ma) overlap extensively with several K-Ar mineral ages reported in Serrano et al. (1996). The zircon ages, moreover, confirm that intrusion of these units took place in the mid-late Miocene, and the young K-Ar ages are therefore not entirely the result of resetting by hydrothermal activity (cf. Serrano et al., 1996). Mine geologists consider the diorite, which occurs as a large, dikelike body within the Cascada granodiorite in the 305 section (Fig. 3B), to have been emplaced later than the granodiorite, a relationship supported by the new zircon ages. On the basis of the U-Pb data, we tentatively propose that, at least in the mine area, the San Francisco batholith was emplaced in at least two separate stages, at ca. 12 Ma (the Río Blanco granodiorite) and ca. 8.4 to 8.2 Ma (Cascada granodiorite and diorite). We regard the available geochronologic evidence for earlier intrusive activity as ambiguous. The younger mid-late Miocene intrusive events apparently occurred shortly before the initiation of hydrothermal activity and the earliest recorded intrusion of a late porphyry unit.

Late porphyries: The zircon U/Pb ID-TIMS ages for three members of the late porphyry complex establish the age of emplacement of the porphyritic dacitic to rhyodacitic hypabyssal intrusions exposed in the mine area. Whereas these rocks have yielded K-Ar ages, largely for biotite, ranging from 5.2 ± 0.3 to 3.9 ± 0.7 Ma, as noted previously, only one of the new zircon ages, that for Don Luis porphyry, falls in this interval. It is now evident that intrusion of quartz monzonite porphyry dike swarms in the area of the Río Blanco underground mine (Serrano et al., 1996; Fig. 3A) was underway by 6.32 Ma, at least 1 m.y. prior to the 5.2 ± 0.12 Ma $^{40}Ar/^{39}Ar$ plateau age reported for K-feldspar in Serrano et al. (1996), implying that the latter records either protracted cooling or, more probably, resetting of the Ar systematics of the quartz monzonite porphyry or, if the feldspar is hydrothermal, late K metasomatism.

The zircon age for Don Luis porphyry, 5.23 ± 0.07 Ma, is similarly significantly older than the K-Ar ages of the apparently phenocrystic biotite therein (4.03 and 4.7 Ma) or the Ar/Ar age documented for K-feldspar in this unit by Serrano et al. (1996; 4.87 ± 0.37 Ma). No previous ages have been reported for the feldspar porphyry unit. Whereas mine personnel have recently proposed that feldspar porphyry forms the outer part of Don Luis porphyry and that the two porphyries represent a single intrusive unit, the new ID-TIMS zircon ages indicate that Don Luis porphyry is significantly younger than the feldspar porphyry.

Río Blanco dacitic plug: The weighted mean SHRIMP age of 4.92 ± 0.09 Ma determined for zircons from the marginal breccias of the dacite plug indicate that this unit was emplaced shortly after the Don Luis porphyry. The early Pliocene age is in permissive agreement with the biotite K-Ar ages previously reported for units of the La Copa complex (i.e., 4.03–4.9 Ma).

$^{40}Ar/^{39}Ar$ age data

With the exception of the two plateau ages for magmatic biotite in the Río Blanco granodiorite (i.e., 11.59 ± 0.08 and 10.98 ± 0.33 Ma), all incremental-heating and spot-fusion mica and alkali feldspar $^{40}Ar/^{39}Ar$ ages determined in this study fall in a narrow early Pliocene interval (4.37 ± 0.06–5.32 ± 0.27 Ma). The summed Gaussian probability plot of all Ar/Ar ages of this study (Fig. 16) reveals peaks at 5.26, 5.12, 4.6 (ostensibly the major event), and 4.38 Ma. The apparent ages of biotite given by incremental-heating plateau and spot-fusion analyses range from 4.57 ± 0.06 to 5.32 ± 0.27 Ma, an unexpectedly narrow range in view of the variable petrologic contexts and inferred origins of the micas.

Two end-member models could be advanced to explain this concentration of Ar/Ar plateau age data. In the first, the apparently variable origin of the micas is evidence that the

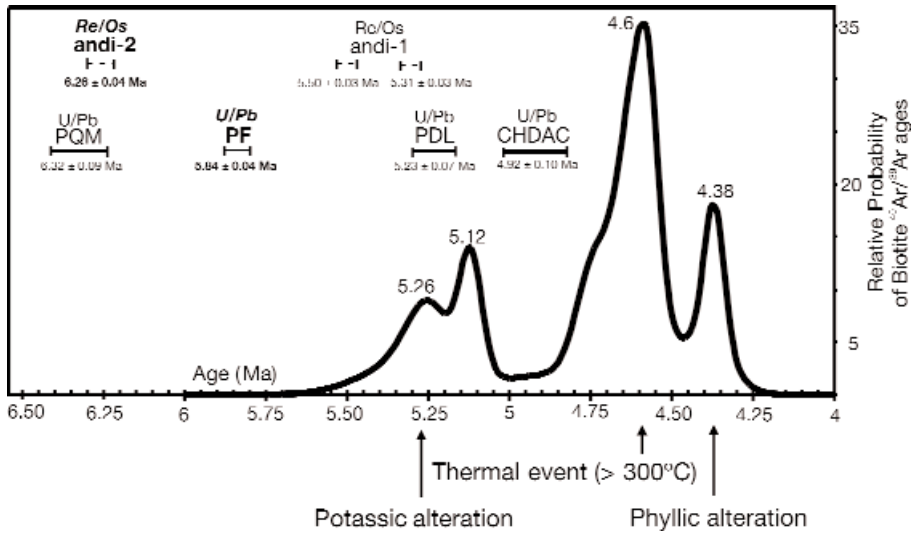

FIG. 16. Summary of new Ar/Ar and U-Pb age data for the Río Blanco, Don Luis, and Sur-Sur sectors (this study), compared to the Re/Os molybdenite ages (dashed lines) of Mathur et al. (2001).

concentration in the biotite ages records either a single or, more probably, several closely spaced thermal events superimposed on earlier formed minerals at a temperature exceeding ca. 300ºC (i.e., sufficient to reset entirely the Ar systematics of the mica, as well as of the single dated K-feldspar). Because such reheating must have occurred after the intrusion of the Don Luis porphyry at 5.23 ± 0.07 Ma, it may only be ascribed to the 4.92 ± 0.09 Ma dacite plug (Figs. 2, 3A) and/or the younger, but apparently more distant, La Copa volcanic complex or rhyolite plug (Fig. 2). In section 155 (Fig. 3A), the dacite plug exhibits a downward-tapering, funnel-like form but, together with the much larger rhyolite plug unit to the north, would have represented a major late-stage heat source in close proximity to the Río Blanco sector of the deposit. Moreover, the variable petrology of the igneous matrix of the La Copa complex suggests that it may have been emplaced over a significant interval, perhaps persisting at least to ca. 4.5 Ma. The sericite ages (4.37 ± 0.06 and 4.40 ± 0.15 Ma) would thus be consistent with the locally intense sericitization in the dacite plug. In this model, none of the early Pliocene biotite or K-feldspar Ar/Ar ages would record an original magmatic crystallization or hydrothermal alteration event.

Alternatively, it could be proposed that the majority of the Ar/Ar biotite ages are representative of magmatic crystallization or initial cooling or, in the case of the late porphyry samples, the hydrothermal alteration of phenocrystic biotite. This model is, however, difficult to justify, because none of the dated late porphyry samples, nor the late porphyries in general, exhibit evidence of penetrative biotitization (Serrano et al., 1996). Furthermore, the late porphyry-hosted biotite yields ages which are unacceptably young in relationship to the correlative zircon ages.

In view of the overlap between the youngest of the late porphyries (Don Luis porphyry: 5.23 ± 0.07 Ma, feldspar porphyry: 5.84 ± 0.04 Ma) and the oldest of the Ar/Ar ages for unambiguously hydrothermal assemblages, namely biotite veins at 5.32 ± 0.27 Ma and K-feldspar veins at 5.25 ± 0.13 Ma, both hosted by the Cascada granodiorite, we propose a model in which potassic alteration, brecciation, and Cu-Mo mineralization overlapped temporally with the intrusion of, at least, the younger of the late porphyry bodies (i.e., feldspar porphyry and Don Luis porphyry). This model is supported by the crosscutting relationships of feldspar porphyry and tourmaline breccia observed by Frikken (2004, p. 80) in a drill hole beneath the Don Luis sector. He notes that "ductile deformation and decreasing grain size of plagioclase feldspar in the Feldspar Porphyry (chilled margin?) imply that crystallization of feldspar porphyry was incomplete at the time these two rocks were brought into contact." On the other hand, he records biotitized magmatic breccia clasts entrained in feldspar porphyry in the Río Blanco sector. These observations do not contradict the temporal overlap of brecciation, Cu-Mo mineralization, and porphyry emplacement proposed above, but we emphasize that the history of alteration and mineralization should be established in each mine sector prior to correlation between sectors.

The $^{40}Ar/^{39}Ar$ spot-fusion age data for unambiguously hydrothermal minerals remain problematic, but we tentatively propose that they indicate that high-grade Cu-Mo mineralization and biotitic alteration of units of the San Francisco batholith occurred during the intrusion of the late porphyry complex and was underway at least by 5.32 ± 0.27 Ma, the weighted mean age of veinlet biotite hosted by the Cascada granodiorite. The main cluster of Ar/Ar ages, predominantly for late porphyry-hosted biotite, in the range 4.75 ± 0.10 to 4.57 ± 0.06 Ma, as well as the 4.6 Ma probability maximum, strongly suggests widespread resetting of the Ar systematics following the intrusion of the dacite plug and probably during the emplacement of the associated units of the La Copa complex (rhyolite plug).

This model for the Río Blanco-Los Bronces district departs from that proposed by both Serrano et al. (1996) and Frikken (2004), who emphasize that the major orebodies in the Río Blanco mine sector are cut by quartz monzonite porphyry and that chalcopyrite in that intrusive unit records remobilization of earlier mineralization.

Discussion

The high-resolution U-Pb zircon and $^{40}Ar/^{39}Ar$ biotite, K-feldspar, and sericite ages presented herein for the Río Blanco, Don Luis, and Sur-Sur sectors of the Río Blanco-Los Bronces porphyry complex define critical aspects of the age relationships but are not unambiguous. The results highlight the uncertainties inherent in the interpretation of Ar-based age data in such enormous magmatic-hydrothermal systems and demonstrate the utility of the independent Re-Os technique.

Local age relationships

The geochronologic data, considered as a whole, provide no direct support for the occurrence of major Cu-Mo mineralization and/or biotitic alteration prior to the intrusion of the oldest dated late porphyry body, the 6.32 ± 0.09 Ma quartz monzonite porphyry. The considerably older, 14.14 ± 0.06 (biotite) and 14.15 ± 0.34 (hornblende) Ma $^{40}Ar/^{39}Ar$ ages reported for matrix minerals in breccias associated with magnetite-amphibole-plagioclase alteration-mineralization at Los Bronces (Skewes et al., 2003) imply that this large-scale, but essentially barren, event occurred prior to the emplacement of the Río Blanco granodiorite. It therefore probably had no direct genetic relationship with the main Cu-Mo ore formation. The $^{40}Ar/^{39}Ar$ ages for both hydrothermal and magmatic biotite in the Río Blanco, Don Luis, and Sur-Sur sectors are in permissive agreement with a broad temporal overlap between ore formation and the emplacement of the feldspar porphyry (5.84 ± 0.04 Ma) and the Don Luis porphyry (5.23 ± 0.07 Ma) intrusions, albeit with major and widespread thermal resetting, plausibly caused by the 4.92 ± 0.09 Ma Río Blanco dacite or, more probably, its associated stocks and diatremes. This hydrothermal chronology is supported, in part, by the duplicate 5.50 ± 0.03 and 5.31 ± 0.03 Ma Re-Os molybdenite ages of Mathur et al. (2001). The dated molybdenites occur in two late hydrothermal breccia bodies hosted by the "Río Blanco granodiorite" on level 12 (ca. 3,450 m). An older, 6.26 ± 0.04 Ma, molybdenite age overlaps in error with the zircon age of quartz monzonite porphyry, indicating that significant Mo mineralization was not, as proposed by Frikken (2004), limited to a single paragenetic stage (7), younger than the emplacement of all three late porphyry intrusive units. The terminal hydrothermal event recorded by the $^{40}Ar/^{39}Ar$ data is the phyllic alteration of Don Luis porphyry at 4.37 ± 0.06 Ma, considerably younger than the dacite plug body but significantly older than the 4.03 ± 0.19 Ma K-Ar biotite age determined for the La Copa rhyolite by Quirt et al. (1971).

We conclude that Cu-Mo mineralization, at least in the Río Blanco, Don Luis, and Sur-Sur sectors, occurred during the emplacement of the late porphyry suite, which therefore was strictly intramineralization. Ore formation was probably initiated during or immediately following intrusion of the quartz monzonite porphyry and probably continued at least to the time of emplacement of the Don Luis porphyry. Whereas the concentration of Ar/Ar biotite ages shortly after the development of the dacite plug complex may be evidence for thermal resetting, we cannot exclude a direct mineralizing role for that unit or the possibility of ore formation at the time of its emplacement. Despite the inconsistency of the $^{40}Ar/^{39}Ar$ and Re-Os ages for, respectively, hydrothermal biotite and/or K-feldspar, and molybdenite, these data support the persistence of potassic alteration and mineralization over an interval of ca. 1.5 m.y., followed by late-stage hydrolytic alteration and further weak mineralization. Our geochronologic data cannot eliminate the possibility of multiple cycles of potassic followed by sericite-quartz alteration or discriminate between models invoking episodic or quasicontinuous mineralization. Analytical imprecision means that the apparent bimodal grouping of the three Re-Os ages of Mathur et al. (2001) is also insufficient evidence for two distinct episodes of molybdenite deposition separated by several hundreds of thousands of years.

Despite these uncertainties, our demonstration that Cu-Mo mineralization overlapped with multiple phases of the late porphyry suite implies that the ore zones similarly developed through multiple episodes of fragmentation and potassic and later hydrolytic alteration.

Regional age relationships

We propose that economic copper mineralization at Río Blanco-Los Bronces commenced in the latest Miocene and continued into the early Pliocene (i.e., from ca. 6.3 to 4.3 Ma). It is therefore probable that much of the Cu in the deposit was introduced broadly contemporaneously with the mineralization episodes inferred for El Teniente (i.e., 5.89, 4.96–5.01, 4.80–4.89, and 4.70 Ma: Cannell et al., 2005). Further, the late-stage sericitic alteration and associated, ostensibly weak, Cu-bearing polymetallic mineralization at Río Blanco-Los Bronces may have coincided temporally with the problematic, ca. 4.42 Ma, chalcopyrite-molybdenite deposition event reported at El Teniente (Mathur et al., 2001). These two enormous deposits, therefore, not only exhibit numerous striking similarities in their anatomy and evolution but were emplaced essentially simultaneously. We therefore conclude that, following the late Miocene development of the Los Pelambres-El Pachón porphyry system at Latitude 32° S (Fig. 1; ca. 10.4–10.8 Ma: Mathur et al., 2001; ca. 11.1–11.2 Ma: Bertens et al., 2003), the domain of intense mineralization in this major belt was displaced southward, expanding to encompass a transect extending at least from ca. 33° S to 34° S.

In this context, it is significant that, on the basis of the K-Ar data of Quirt et al. (1971), it has been argued (Skewes et al., 2002, p. 306) that a systematic southward migration of porphyry Cu emplacement over the late Miocene-early Pliocene interval directly reflected the "southward sweep of the locus of subduction of the Juan Fernández Ridge (Yañez et al., 2001)." The ensuing transition to flat subduction is considered by Skewes et al. (2002) to be further recorded by the diachronous termination of frontal-arc magmatism at ca. 6 Ma in the Los Pelambres area, through ca. 3.9 Ma at the latitude of Río Blanco, to ca. 1.8 Ma in the El Teniente transect. Kay and Mpodozis (2002, p. 52), however, observed that mineralization at El Teniente occurred "outside of a 200 km swath from the ridge center" and was, therefore, unlikely to have been directly influenced by its subduction. In a comprehensive review of the distribution of magmatic activity in the southern central Andes relative to the southward migration of the locus of subduction of the Juan Fernández Ridge, they

argue that the inception of flat subduction and arc perturbation was determined fundamentally by larger scale convergence relationships at the margin of the South American plate. Our demonstration that Cu-Mo mineralization was sensibly simultaneous at Río Blanco and El Teniente may similarly imply that the development of these enormous porphyry copper centers was only indirectly related to the process of ridge subduction which, by 6 to 7 Ma, exhibited a rate of southward migration not exceeding ca. 25 km/m.y. (Yañez et al., 2001).

Concluding Statement

Rigorous clarification of the age relationships of hydrothermal activity and shallow intrusion in world-class porphyry systems will require, at the least, detailed U-Pb, $^{40}Ar/^{39}Ar$, and Re-Os age determinations. These techniques are sensitive to entirely different geologic processes and hence provide mutual support and constraints. Whereas the U-Pb and Ar/Ar databases at Río Blanco-Los Bronces are extensive, except for the late-stage events, further Re-Os dating of molybdenite from well constrained paragenetic contexts would be valuable, despite the difficulties inherent in the Re-Os systematics of young molybdenites (Košler et al., 2003). We interpret our geochronologic data as evidence that economic mineralization overlapped in time with late porphyry emplacement, in contrast to the conclusions of Serrano et al. (1996) and the recent work of Frikken (2004). Similarly, Maksaev et al. (2002) and Skewes et al. (2002) recognized the temporal coincidence of Cu-Mo mineralization and felsic magmatism at El Teniente, although the former do not address the genetic relationships implicit in this relationship, and the latter argue against a direct connection. With regard to the Río Blanco deposit, we suggest that the spatial juxaposition of altered host rocks and porphyry may not possess the temporal significance generally assigned to it. In this case, batches of rhyodacitic melt that rose together with hydrothermal fluids from a deeper zone in the roof of the parental pluton may have been mutually exclusive in mechanical terms in the ore-forming environment. The water-rock interaction and fragmentation required for alteration and mineralization would not be possible in the bodies of melt until they had crystallized and extensively cooled but would be focused in cool, reactive preexisting rocks. Thus, the melts provided thermal energy for the upward propulsion of the mineralizing brines but were not in themselves productive (i.e., were not the immediate source of the fluids or ore metals). In this context, it is significant that Davidson and Kamenetsky (2001) and Davidson et al. (2005) have demonstrated that fluid inclusions in the La Copa complex indicate that the parental magma chamber remained potentially fertile until its terminal stages. These findings are compatible with the new geochronologic data which demonstrate extensive temporal overlap between high-grade Cu-Mo mineralization and felsic late porphyry emplacement.

Acknowledgments

The authors thank the Andina Division of CODELCO Chile for funding this investigation and for permitting its publication. The good offices and unstinting support of Luis Serrano, Administrator of Exploration and Mineral Resources, were a prerequisite for initiation and completion of the research. Andina Division geologists Augusto Mont and Humberto Ortega are particularly thanked for their help in sampling and for their geologic discussions. Robert Duncan, Oregon State University, and Samuel Bowering, Massachusetts Institute of Technology, carried out the geochronological analytical work. At the Universidad de Chile, Juan Vargas is thanked for his help in mineral separation and Mauricio Belmar for taking the BSE biotite single grain image and Nilanjan Chatterjee, Massachusetts Institute of Technology, for taking the BSE biotite thin section photos.

The paper has benefited from discussions with CODELCO Chile geologist Enrique Tidy. The SHRIMP analysis and BSE photos were financed through Chilean grant DID I-04-2/2001. We gratefully acknowledge Joan Charbonneau's endless but uncomplaining typing of the manuscript. A.H.C. thanks the Natural Sciences and Engineering Research Council of Canada for their support of the Queen's University Central Andean Metallogenetic Project, of which this study is a component. We also thank Fred McDowell, University of Texas, and David Cooke, CODES, University of Tasmania, for providing insightful and constructive reviews of this manuscript. Mark Hannington, the editor, carefully checked the revised text and figures.

August 4, 2004; July 15, 2005

REFERENCES

Arancibia, O.N., and Clark, A.H., 1995, Early magnetite-amphibole-plagioclase alteration-mineralization in the Island Copper porphyry copper-gold-molybdenum deposit, British Columbia: Economic Geology, v. 91, p. 402–438.

Bertens, A., Deckart, K., and Gonzalez, A., 2003, Geocronología U-Pb, Re-Os y $^{40}Ar/^{39}Ar$ del pórfido de Cu-Mo Los Pelambres, Chile Central: Congreso Geológico Chileno, X, Concepción, Chile, 2003, 5 p. (CD-ROM).

Blondel, J.R., 1980, Pórfido de composición granodiorítica de la mina Río Blanco: Unpublished Memoria de Título, Departamento de Geología, Universidad de Chile, Santiago, 88 p.

Blondel, J.R., Stambuk, V., and Galeb, M., 1988, Cuerpos subvolcánicos dacíticos asociados al yacimiento Río Blanco: Congreso Geológico Chileno, V, Santiago, Actas, v. 1, p. B475–B489.

Cannell, J., Cooke, D.R., Stein, H.J., and Markey, R., 2005, New paragenetically constrained Re-Os molybdenite ages for the El Teniente Cu-Mo porphyry deposit, central Chile: Economic Geology, v. 100, p. 979–1003.

Clark, A.H., 1993, Are outsize porphyry copper deposits either anatomically or environmentally distinctive: Society of Economic Geologists Special Publication 2, p. 213–283.

Clark, A.H., Archibald, D.A., Lee, A.W., Farrar, E., and Hodgson, C.J., 1998, Laser probe $^{40}Ar/^{39}Ar$ ages of early- and late-stage alteration assemblages, Rosario porphyry copper-molybdenum deposit, Collahuasi district, I región, Chile: Economic Geology, v. 93, p. 326–337.

Davidson, P., and Kamenetsky, V.S., 2001, Immiscibility and continuous felsic melt-fluid evolution within the Río Blanco porphyry system, Chile: Evidence from inclusions in magmatic quartz: Economic Geology, v. 96, p. 1921–1929.

Davidson, P., Kamenetsky, V.S., Cooke, D.R., Frikken, P., Hollings, P., Ryan, C, Van Achterbergh, E., Mernagh, T., Skarmeta, J., Serrano, L., and Vargas, R, 2005, Magmatic precursors of hydrothermal fluids at the Rio Blanco Cu-Mo deposit, Chile: Links to silicate magmas and metal transport: Economic Geology, v. 100, p. 963–978.

Frikken, P.H., 2004, Breccia-hosted copper-molybdenum mineralisation at Río Blanco, Chile: Unpublished Ph.D. thesis, Hobart, CODES, University of Tasmania, 248 p.

Frikken, P.H., Cooke, D.R., Walshe, J.L., Archibald, D., Skarmeta, J., Serrano, L., and Vargas, R., 2005, Mineralogical and isotopic zonation in the Sur-Sur tourmaline breccia, Río Blanco-Los Bronces Cu-Mo deposit, Chile—implications for ore genesis: Economic Geology, v. 100, p. 935–961.

Gustafson, L.B., Orquera, W., McWilliams, M., Castro, M., Olivares, O., Rojas, G., Maluenda, J., and Mendez, M., 2001, Multiple centers of mineralization in the Indio Muerto district, El Salvador, Chile: Economic Geology, v. 96, p. 325–350.

Harrison, T.M., Duncan, I., and McDougall, I., 1985, Diffusion of ^{40}Ar in biotite: Temperature, pressure and compositional effects: Geochimica et Cosmochimica Acta, v. 49, p. 2461–2468.

Hollings, P., Cooke, D., and Clark, A.H., 2005, Regional geochemistry of Tertiary volcanic rocks in Central Chile: Implications for the tectonic setting of giant porphyry copper and epithermal deposit genesis: Economic Geology, v. 100, p. 887–904.

Kay, S., and Mpodozis, C., 2001, Central Andean ore deposits linked to evolving shallow subduction systems and thickening crust: GSA Today, v. 11, no. 3, p. 4–9.

——2002, Magmatism as a probe to the Neogene shallowing of the Nazca plate beneath the modern Chilean flat-slab: Journal of South American Earth Sciences, v. 15, p. 39–57.

Kay, S., Orrel, S., and Abbruzzi, J.M., 1996, Zircon and whole rock Nd-Pb isotopic evidence for a Grenville age and a Laurentian origin for the basement of the Precordillera in Argentina: Journal of Geology, v. 104, p. 637–648.

Kay, S., Mpodozis, C., and Coira, B., 1999, Magmatism, tectonism, and mineral deposits of the central Andes (22º–33 ºS): Society of Economic Geologists Special Publication 7, p. 27–59.

Košler, J., Simonetti, A., Sylvester, P.J., Cox, R.A., Tubrett, M.N., and Wilton, D.M.C., 2003, Laser-ablation ICP-MS measurements of Re/Os in molybdenite and implications for Re-Os geochronology: Canadian Mineralogist, v. 41, p. 307–320.

Kusakabe, M., Hori, M., and Matsuhisa, Y., 1990, Primary mineralization-alteration of the El Teniente and Río Blanco porphyry copper deposits, Chile: Stable isotope, fluid inclusion and $Mg^{+2}/Fe^{+2}/Fe^{+3}$ ratios of hydrothermal fluids, *in* Herbert, H.K., and Ho, S.E., eds., Stable isotopes and fluid processes in mineralization: Perth, University of Western Australia Press, p. 244–259.

Love, D.A., Clark, A.H., Hodgson, C.J., Mortensen, J.K., Archibald, D.A., and Farrar, E., 1998, The timing of adularia-sericite-type mineralization and alunite-kaolinite-type alteration, Mount Skukum epithermal gold deposit, Yukon Territory, Canada: $^{40}Ar/^{39}Ar$ and U-Pb geochronology: Economic Geology, v. 93, p. 437–462.

Ludwig, K.R., 1980, Calculation of uncertainties of U-Pb isotopic data: Earth and Planetary Science Letters, v. 4, p. 212–220.

——1999, User's manual for Isoplot/Ex, Version 2.10, A geochronological toolkit for Microsoft Excel: 1a.

——2000, SQUID 1.00, A user's manual: Berkeley, CA, Berkeley Geochronological Center Special Publication 2.

Maksaev, V., Munizaga, F., McWilliams, M., Fanning, M., Mathur, R., Ruiz, J., and Thiele, K., 2002, El Teniente porphyry copper deposit in the Chilean Andes: New geochronological time frame and duration of hydrothermal activity [abs.]: Geological Society of America Abstracts with Programs, v. 34, p. 336.

Mathur, R, Ruiz, J.R., and Munizaga, F.M., 2001, Insights into Andean metallogenesis from the perspective of Re-Os analyses of sulphides [abs.]: SERNAGEOMIN, III. South American Symposium on Isotope Geology, Santiago, Sociedad Geológica de Chile 2001, p. 500–503. (CD-ROM).

Paces, J.B., and Miller, J.D., 1993, Precise U-Pb ages of Duluth Complex and related mafic intrusions, northeastern Minnesota: Geochronological insights to physical, petrogenetic, paleomagnetic, and tectonomagmatic process associated with the 1.1 Ga Midcontinent rift system: Journal of Geophysical Research, v. 98, p. 13,997–14,013.

Parrish, R., Roddick, J.C. Loveridge, W.D., and Sullivan, R.W., 1987, Uranium-lead analytical techniques at the geochronology laboratory, Geological Survey of Canada: Geological Survey of Canada Paper 87–2, p. 3–7.

Quirt, G.S., 1972, A potassium-argon geochronological investigation of the Andean mobile belt of north-central Chile: Unpublished Ph.D. thesis, Kingston, Ontario, Canada, Queen's University, 240 p.

Quirt, G.S., Clark, A.H., Farrar, E., and Sillitoe, R.H., 1971, Potassium-argon ages of porphyry copper deposits in northern and central Chile: Economic Geology, v. 67, p. 980–981.

Reynolds, P., Ravenhurst, C., Zentilli, M., and Lindsay, D., 1998, High-precision $^{40}Ar/^{39}Ar$ dating of two consecutive hydrothermal events in the Chuquicamata porphyry copper system, Chile: Chemical Geology, v. 148, p. 45–60.

Richards, J.P., Noble, S.R., and Pringle, M.S., 1999, A revised late Eocene age for porphyry Cu magmatism in the Escondida area, northern Chile: Economic Geology, v. 94, p. 1231–1248.

Rivano, S., Godoy, E., Vergara, M., and Villaroel, R., 1990, Redefinición de la Formación Farellones en la Cordillera de los Andes de Chile Central (32–34ºS): Revista Geológica de Chile, v. 17, p. 205–214.

Roddick, J.C., 1987, Generalized numerical error analysis with application to geochronology and thermodynamics: Geochimica et Cosmochimica Acta, v. 51, p. 2129–2135.

Rojas, A., 1985, Geología y petrogénesis del pórfido Don Luis en el yacimiento Río Blanco, CODELCO-Chile: Departamento de Geología y Geofísica, Universidad de Chile, Santiago, Unpublished Memoria de Título, 109 p.

Serrano, L., Vargas, R., Stambuk, V., Aguilar, C., Galeb, M., Holmgren, C., Contreras, A., Godoy, S., Vela, L., Skewes, M.A., and Stern, C.R., 1996, The late Miocene to early Pliocene Río Blanco-Los Bronces copper deposit, central Chilean Andes: Society of Economic Geologists Special Publication 5, p. 119–130.

Sillitoe, R., 1988, Epochs of intrusion-related copper mineralization in the Andes: Journal of South American Earth Sciences, v. 1, p. 89–108.

Skewes, A., and Holmgren, C., 1993, Solevamiento andino, erosión y emplazamiento de brechas mineralizadas en el depósito de cobre porfídico Los Bronces, Chile Central (33ºS): Aplicación de termometría de inclusiones fluidas: Revista Geológica de Chile, v. 20, p. 71–84.

Skewes, A., Holmgren, C., and Vargas, R., 1994, Alteración a anfíbola y magnetita en el megayacimiento Río Blanco-Los Bronces, Chile Central: Congreso Geológico de Chile, VII, Concepción, Actas, v. 1, p. 1623–1626.

Skewes, M.A., and Stern, C.R., 1995, Genesis of the giant late Miocene to Pliocene copper deposits of central Chile in the context of Andean magmatic and tectonic evolution: International Geology Review, v. 37, p. 71–84.

——1996, Late Miocene mineralized breccias in the Andes of Central Chile: Sr and Nd isotopic evidence for multiple magmatic sources: Society of Economic Geologists Special Publication 5, p. 33–41.

Skewes, M.A., Arévalo, A., Floody, R., Zúñiga, H., and Stern, C.R., 2002, The giant El Teniente breccia deposit: Hypogene copper distribution and emplacement: Society of Economic Geologists Special Publication 9, p. 299–332.

Skewes, M.A., Holmgren, C., and Stern, C.R., 2003, The Donoso copper-rich, tourmaline-bearing breccia pipe in central Chile: Petrologic, fluid inclusion and stable isotope evidence for an origin from magmatic fluids: Mineralium Deposita, v. 38, p. 2–21.

Spröhnle, C., 1988, Geología de los sectores Sur-Sur y Don Luis del yacimiento Río Blanco, División Andina, CODELCO-Chile: Departamento de Geología y Geofísica, Universidad de Chile, Santiago, Unpublished Memoria de Título, 177 p.

Stacey, J.S., and Kramer, J.D., 1975, Approximation of terrestrial lead isotope evolution by a two-stage model: Earth and Planetary Science Letters, v. 26, p. 207–221.

Stambuk, V., Serrano, L., and Vargas, R., 1985, Geología del sector Sur-Sur, yacimiento Río Blanco: Congreso Geológico Chileno, IV, Antofagasta, Actas, v. 2, p. 383–404.

Steiger, R.H., and Jäger, E., 1977, Subcomission on geochronology: Convention on the use of decay constants in geo- and cosmo-chronology: Earth and Planetary Science Letters, v. 36, p. 359–362.

Tera, F., and Wasserburg, G.J., 1972, U-Th-Pb systematics in three Apollo 14 basalts and the problem of initial Pb in lunar rocks: Earth and Planetary Science Letters, v.14, p. 281–304.

Vargas, R., Gustafson, L.B., Vukasovic, M., Tidy, E., and Skewes, M.A., 1999, Ore breccias in the Río Blanco-Los Bronces porphyry copper deposit, Chile: Society of Economic Geologists Special Publication 7, p. 281–297.

Vergara, M., and Drake, R., 1978, Edades potasio-argón y su implicancia en la geología regional de Chile: Departamento de Geología, Facultad de Ciencias Físicas y Matemáticas, Universidad de Chile, Santiago, Comunicaciones, p. 1–11.

——1979, Eventos magmáticas-plutónico en los Andes de Chile Central: Segundo Congreso Geológico Chileno, Arica, Actas, v. 1, p. F19–F30.

Vergara, M., and Latorre, J., 1984, El complejo volcánico pliocénico de Río Blanco, Santiago: Revista Geológica de Chile, no. 22, p. 49–60.

Vergara, M., Charrier, R., Munizaga, F., Sepúlveda, P., Thiele, R., and Drake, R., 1988, Miocene volcanism in the Central Chilean Andes (31º30'–34º35'S): Journal of South American Earth Sciences, v. 1, p. 199–209.

Warnaars, F.W., Holmgren, C., and Barassi, S., 1985, Porphyry copper and tourmaline breccias at Los Bronces-Río Blanco, Chile: ECONOMIC GEOLOGY, v. 80, p. 1544–1565.
Whiting, B.H., Hodgson, C.J., and Mason, R., eds., 1993, Giant ore deposits: Society of Economic Geologists Special Publication 2, 404 p.
Williams, I.S., 1998, U-Th-Pb geochronology by ion microprobe: Reviews in Economic Geology, v. 7, p. 1–35.
Yáñez, G, Ranero, C.R., von Huene, R., and Díaz, J., 2001, Magnetic anomaly interpretation across the southern central Andes (32º–34ºS): The role of the Juan Fernández Ridge in the late Tertiary evolution of the margin: Journal of Geophysical Research, v. 106, p. 6325–6345.
Zentilli, M., Pop, N., Heaman, L., and Boric, R., 2001, Evidence of Proterozoic crust under the Coastal Cordillera of Central Chile: Grenville age xenocrystic zircons in Cretaceous volcanic rocks [abs.]: SERNAGEOMIN, III. South American Symposium on Isotope Geology, Santiago, Sociedad Geológica de Chile 2001, p. 642. (CD-ROM)

Appendix 1

Analytical Procedures

The ages of most of the igneous units exposed in the Río Blanco and Sur-Sur areas of the district are herein established through ID-TIMS U-Pb dating of zircons, as well as a single SHRIMP date, providing a robust framework for the interpretation of new $^{40}Ar/^{39}Ar$ ages obtained by laser-induced step heating and spot fusion of hydrothermal minerals from the eastern part of this extensive mineralized domain. Samples of host rocks and ore assemblages were selected from drill core and underground exposures by the senior author with the advice and assistance of CODELCO-Andina mine geologist Augusto Mont.

For conventional and single-zircon grain TIMS U-Pb analysis, magmatic zircons were separated from ca. 8- to 10-kg samples using standard crushing, grinding, Wilfley Table, heavy liquid (methylene iodide), and Frantz magnetic separation methods. At the geochronological laboratory of the University of British Columbia, Vancouver, the lowest magnetic susceptibility fractions were handpicked for zircons based on grain size and morphology. Large fractions were obtained to ensure that sufficient radiogenic Pb was available for analysis. Zircon dissolution and Pb and U separation and purification were carried out following procedures modified after those of Parrish et al. (1987). Zircons were washed in dilute nitric acid, spiked with a mixed $^{233-235}$ U-^{205}Pb tracer, and then dissolved in Savilex bombs. U and Pb were separated and purified in ion exchange columns and loaded, together with a mixed silica gel-phosphoric acid emitter, on outgassed Re filaments. Isotopic compositions were measured using a Daly detector in peak-switching mode on a modified VG-54R mass spectrometer. Measured Pb isotope ratios were corrected for mass discrimination of 0.37 ± 0.07 percent/amu based on replicate analyses of the NBS Pb standard S.R.M. 981. During this study, detector blanks were 2 to 3 pg for Pb and 1 pg for U. Errors attached to individual analyses were calculated using the numerical error propagation method of Roddick (1987). Decay constants are those recommended by Steiger and Jäger (1977). The model of Stacey and Kramer (1975) was used to estimate the composition of initial common Pb. Regression of discordant data arrays employed a modified version of the York-II model. Intercept ages were calculated using the Ludwig (1980) algorithm and multiplied by MSWD in order to allow for excess scatter in the data (Parrish et al. 1987). All errors are quoted at the 2σ level.

TIMS U-Pb analysis of single zircon grains from two samples were carried out at the Thermal Ionization Mass Spectrometer Laboratory at the Massachusetts Institute of Technology, using techniques similar to those employed for zircon separates. Isotopic compositions were measured by using a Daly detector in ion-counting mode which allows for precise measurement of low signals on a fully automated VG Sector 54 thermal ionization mass spectrometer. Due to extremely low chemistry blanks, total analytical blanks during analyses were less than 0.6 pg of Pb and less than 0.1 pg U. High-precision U-Pb dating of young single zircons or zircon fragments can be carried out with radiogenic Pb concentrations as low as 40 pg. Common-Pb corrections were calculated by using the model of Stacey and Kramer (1975) and the interpreted age of the sample.

For SHRIMP U-Pb dating, handpicked zircons were mounted in epoxy together with FC1 and SL13 zircon standards, cut in half, and polished. Reflected and transmitted light photographs and cathdoluminescence SEM pictures were taken of all zircons to obtain information on the internal structures of the grains and to target specific areas therein. U, Th, and Pb analyses were carried out using SHRIMP II at the Australian National University. Data were reduced as described by Williams (1998, and references therein), using the SQUID Excel Macro program of Ludwig (2000). U/Pb ratios were normalized relative to a value of 0.1859 for the $^{206}Pb/^{238}U$ ratio of the 1099 Ma FC1 standard zircon (Paces and Miller, 1993). Uncertainties for individual analyses (ratios and ages) are given at the 1σ level, whereas uncertainties in calculated weighted mean ages are reported at 2σ. The Tera and Wasserburg (1972) Concordia plot, relative probability plot with stacked histogram, and weighted mean $^{206}Pb/^{238}U$ age calculations were carried out using the ISOPLOT/EX program of Ludwig (1999).

For $^{40}Ar/^{39}Ar$ incremental-heating geochronology, high-quality separates of apparently igneous and hydrothermal biotite were prepared by crushing, sieving, and handpicking under a binocular microscope. In addition, six small rock tablets of mineralized samples, incorporating two each of early biotite, K-feldspar, and quartz-sericite veins, were prepared for in situ spot total-fusion analysis, a technique that yields a date comparable to a conventional K-Ar analysis but provides better paragenetic control, in this case by excluding grains of magmatic minerals (Clark et al., 1998). Single-grain samples were wrapped in ultra-pure Cu foil and inserted with the unwrapped rock tablets, together with the Fish Canyon flux monitor FCT-3 (28.04 ± 0.12 Ma), into a glass vial, which was pumped down to 10^{-4} Torr and then sealed, to avoid contact with the reactor cooling water during the irradiation procedure. The vial was irradiated for 6 h in the IMW TRIGA experimental nuclear reactor at Oregon State University, Corvallis. The samples were then extracted and unwrapped and loaded into a Cu planchett. Incremental heating of the biotite separates and spot-heating of the rock tablets (2 min for each spot) were carried out using a CO_2 laser connected to a MAP250/50 mass spectrometer. The heating temperature was controlled by the use of an optical pyrometer and by the laser power. For step-heating analyses, an initial heating increment at 400ºC was pumped away, on the assumption that the extracted gas largely represents surface argon. The Ar/Ar dates are herein quoted at 2σ error intervals as external errors, incorporating the analytical error, the error of the flux monitor and that of the decay constants (after Steiger and Jäger, 1977).

APPENDIX 2A. U-Pb Analytical Data for Zircon Fractions

Sample Description[1]	Wt (mg)	U (ppm)	Pb[2] (ppm)	$^{206}Pb/^{204}Pb$[3] (meas.)	Total common Pb (pg)	% ^{208}Pb[3]	$^{206}Pb/^{238}U$[4] (±% 1σ)	$^{207}Pb/^{235}U$[4] (±% 1σ)	$^{207}Pb/^{206}Pb$[4] (±% 1σ)	$^{206}Pb/^{238}U$ age (Ma; ±% 2σ)	$^{207}Pb/^{235}U$ age (Ma; ±% 2σ)	$^{207}Pb/^{206}Pb$ age (Ma)
						Andesite-Nivel 16						
A: N2.134-149.s	0.025	462	1.42	359	6	22.1	0.00267(0.22)	0.01703(2.31)	0.04634(2.23)	17.16(0.08)	17.15(0.78)	15.5
B: N2.104-134.s	0.081	257	0.74	133	30	16.3	0.00268(0.38)	0.01712(4.63)	0.04635(4.41)	17.25(0.13)	17.24(1.58)	15.6
C: N2.104-134.s	0.034	361	1.13	188	12	23.0	0.00268(0.39)	0.01711(4.02)	0.04628(3.88)	17.26(0.13)	17.23(1.37)	12.0
D: N2. 104-134.s	0.027	504	1.62	290	8	25.0	0.00267(0.26)	0.01714(3.12)	0.04649(3.58)	17.21(0.09)	17.26(1.27)	23.2
						Andesite-PZ-2007						
A: N10.+180.s	0.135	427	1.21	74	164	17.2	0.00261(0.76)	0.01667(9.13)	0.04641(8.76)	16.77(0.25)	16.79(3.04)	18.8
B: N10.+180.s	0.105	283	0.88	34	285	21.8	0.00265(2.12)	0.02188(7.04)	0.05991(5.87)	17.05(0.72)	21.97(3.06)	600.4
C: N10. 134-180.s	0.079	728	2.04	140	75	16.1	0.00261(0.36)	0.01670(3.54)	0.04635(3.37)	16.83(0.12)	16.82(1.18)	15.6
D: N10. 134-180.s	0.114	265	0.73	104	55	16.7	0.00255(0.56)	0.01632(2.92)	0.04637(2.65)	16.43(0.18)	16.44(0.95)	16.9
E: N10. 104-134.s	0.213	439	1.23	122	139	19.6	0.00250(0.55)	0.01604(1.91)	0.04648(1.59)	16.12(0.18)	16.16(0.61)	22.4
F: N10. 104-134.s	0.090	338	0.95	69	91	20.6	0.00248(0.97)	0.01582(4.75)	0.04636(4.30)	15.94(0.31)	15.94(1.50)	16.2
G: N10. 74-104.s+m	0.054	320	4.93	1239	13	7.9	0.01487(0.09)	0.22338(0.22)	0.10893(0.18)	95.17(0.18)	204.72(0.80)	1781.7
						GDRB						
A: N2-74.e	0.060	274	0.60	126	18	17.6	0.00201(0.49)	0.01311(2.07)	0.04721(1.81)	12.97(0.13)	13.22(0.54)	59.9
B: N2.104-134.e	0.040	353	0.79	68	36	16.7	0.00208(1.10)	0.01424(3.77)	0.04974(1.18)	13.37(0.29)	14.35(1.07)	182.8
C: N2.104-134.s	0.107	394	0.81	153	36	16.7	0.00190(0.42)	0.01217(1.61)	0.04655(1.37)	12.21(0.10)	12.29(0.39)	26.4
D: N2.104-134.s	0.133	352	0.73	46	195	18.8	0.00186(1.67)	0.01186(10.3)	0.04635(9.58)	11.96(0.40)	11.97(2.45)	15.6
E: N2.104-134.s	0.123	384	0.76	157	38	18.0	0.00181(0.35)	0.01161(4.97)	0.04642(4.78)	11.68(0.08)	11.72(1.16)	19.4
F: N2.104-134.s	0.172	458	0.95	98	113	18.7	0.00188(0.71)	0.01206(2.40)	0.04644(1.99)	12.13(0.17)	12.17(0.58)	20.4
						Diorite						
A: N2.+180.s	0.360	119	0.18	80	60	16.3	0.00141(0.90)	0.00891(3.16)	0.04596(2.65)	9.06(0.16)	9.01(0.57)	-4.3
B: N2.+180.e	0.268	209	0.46	320	22	20.0	0.00195(0.23)	0.01285(2.99)	0.04771(2.87)	12.58(0.06)	12.97(0.77)	85.0
C: N2.+180.m	0.190	90	0.13	60	33	19.6	0.00133(1.45)	0.00847(23.8)	0.04628(23.0)	8.55(0.25)	8.57(4.06)	12.4
D: N2.134-149.m	0.291	135	0.20	166	22	16.5	0.00135(0.42)	0.00893(6.53)	0.04798(6.29)	8.69(0.07)	9.02(1.17)	98.1
E: N2.104-134.m	0.199	138	0.21	56	62	17.0	0.00139(1.10)	0.00890(12.6)	0.04630(12.0)	8.98(0.20)	9.00(2.25)	13.5
F: N2.74-104.e	0.213	154	0.24	144	22	20.3	0.00139(0.38)	0.00888(5.54)	0.04635(5.33)	8.95(0.07)	8.97(0.99)	15.6
						PQM						
A: N2.+134.s	0.310	207	0.23	108	42	20.4	0.00098(0.68)	0.00637(10.6)	0.04712(10.2)	6.32(0.09)	6.45(1.36)	55.3
B: N2.+134.s	0.370	229	0.26	249	24	16.0	0.00108(0.40)	0.00718(1.97)	0.04845(1.87)	6.93(0.06)	7.27(0.29)	121.3
C: N2.+134.s	0.288	168	0.24	140	32	16.0	0.00130(0.45)	0.01011(1.41)	0.05644(1.16)	8.37(0.08)	10.21(0.29)	469.7
D: N2.+134.s	0.190	205	0.23	77	42	18.5	0.00103(0.77)	0.00658(11.0)	0.04639(10.7)	6.63(0.10)	6.66(1.46)	18.1
E: N2.74-104.e	0.090	163	0.41	299	7	16.4v	0.00233(0.25)	0.01647(1.60)	0.05130(1.48)	14.99(0.07)	16.58(0.53)	254.1
F: N2.-74.e	0.086	257	0.31	101	17	21.8	0.00106(0.42)	0.00690(2.37)	0.04736(2.14)	6.81(0.06)	6.98(0.33)	67.5
G: N2.+149.s	0.462	193	0.21	133	47	18.7	0.00098(0.53)	0.00628(8.62)	0.04627(8.31)	6.34(0.07)	6.35(1.09)	11.8
						PF						
A: N1.+180.s	0.435	206	0.20	373	14	15.9	0.00090(0.18)	0.00583(2.09)	0.04682(2.00)	5.82(0.02)	5.90(0.25)	40.2
B: N1.+180.s	0.420	243	0.24	559	11	14.9	0.00093(0.20)	0.00608(1.76)	0.04737(1.68)	6.00(0.02)	6.15(0.22)	67.9
C: N1.134-180.s	0.188	269	0.27	210	15	18.6	0.00091(0.29)	0.00587(1.20)	0.04698(1.05)	5.84(0.03)	5.94(0.14)	48.2
D: N1.134-180.s	0.224	258	0.27	303	12	19.2	0.00094(0.24)	0.00610(2.50)	0.04706(2.38)	6.06(0.03)	6.18(0.31)	52.0
E: N1.-74.e	0.051	306	1.56	840	5	16.3	0.00470(0.15)	0.03336(0.55)	0.05151(0.50)	30.21(0.09)	33.32(0.36)	263.6

APPENDIX 2A. *(Cont.)*

Sample Description[1]	Wt (mg)	U (ppm)	Pb[2] (ppm)	$^{206}Pb/^{204}Pb$[3] (meas.)	Total common Pb (pg)	% ^{208}Pb[3]	$^{206}Pb/^{238}U$[4] (±% 1σ)	$^{207}Pb/^{235}U$[4] (±% 1σ)	$^{207}Pb/^{206}Pb$[4] (±% 1σ)	$^{206}Pb/^{238}U$ age (Ma; ±% 2σ)	$^{207}Pb/^{235}U$ age (Ma; ±% 2σ)	$^{207}Pb/^{206}Pb$ age (Ma)
						PDL						
A: N2.+134.s.a	0.625	340	1.51	2566	22	12.1	0.00431(0.09)	0.03097(0.20)	0.05212(0.13)	27.72(0.05)	30.97(0.12)	290.8
B: N2.+134.s.a	0.714	282	0.55	623	37	15.3	0.00181(0.16)	0.01241(0.43)	0.04979(0.34)	11.64(0.04)	12.52(0.11)	185.4
C: N2.+134.s.a	0.724	297	0.49	321	68	13.9	0.00157(0.22)	0.01045(0.70)	0.04824(0.56)	10.12(0.05)	10.55(0.15)	111.2
D: N2.+134.s.a	0.708	296	0.47	539	35	18.7	0.00141(0.17)	0.00961(0.49)	0.04930(0.40)	9.11(0.03)	9.71(0.03)	162.2
E: N1.44-74.e	0.206	348	1.56	1111	17	13.4	0.00428(0.12)	0.03070(0.28)	0.05203(0.21)	27.53(0.07)	27.53(0.07)	286.9
F: N2.-74.e	0.074	318	0.67	340	8	19.6	0.00188(0.19)	0.01314(0.89)	0.05069(0.80)	12.11(0.05)	13.25(0.23)	226.5
G: M2.-104.e	0.094	388	5.92	1358	25	8.4	0.01546(0.12)	0.11210(0.25)	0.05258(0.18)	98.93(0.24)	107.88(0.52)	310.5
H: N2.+149.s	0.192	361	0.32	115	36	16.5	0.00081(0.64)	0.00518(9.87)	0.04624(9.56)	5.23(0.07)	5.24(1.03)	10.0

A bbreviations: GDRB = Río Blanco granodiorite, PDL = Don Luis porphyry, PF = feldspar porphyry, PQM = quartz monzonite porphyry

[1] N1. N2 = nonmagnetic at n degrees side slope on Frantz magnetic separator; grain size given in microns; a = abraded, e = elongate prisms, m = equant multifaceted, s = stubby prismis

[2] Radiogenic Pb; corrected for blank, initial common Pb, and spike

[3] Corrected for spike and fractionation as determined from replicate analyses of NBS common Pb standards

[4] Corrected for 2 pg blank Pb and 1 pg blank U and initial common Pb

APPENDIX 2B. U-Pb Analytical Data for Zircon Single Grains

Sample description	Wt[1] (μg)	U (ppm)	Pb[2] (ppm)	$^{206}Pb/^{204}Pb$[3]	Pb[2,3] (pg)	$^{208}Pb/^{206}Pb$[4]	$^{206}Pb/^{238}U$[4,5] (±% 2σ)	$^{207}Pb/^{235}U$[4,5]	$^{207}Pb/^{206}Pb$[4,5] (± % 2σ)	$^{206}Pb/^{238}U$ age (Ma)	$^{207}Pb/^{235}U$ age (Ma)	$^{207}Pb/^{206}Pb$ age (Ma)
						GDCC						
z1	7.4	71	0.13	76.5	0.9	0.271	0.001618 (3.35)	0.0107	0.04809 (3.52)	10.4	10.8	103.7
z2	9.2	84	0.12	88.8	0.9	0.224	0.001300 (2.75)	0.0084	0.04703 (3.00)	8.4	8.5	50.7
z3	16.1	75	0.12	170.4	0.7	0.260	0.001406 (1.29)	0.0090	0.04653 (3.15)	9.1	9.1	25.1
						Diorite						
z1	2.5	166	0.5	89.3	1.0	0.278	0.002676 (2.7)	0.01711	0.04637 (2.7)	17.2	17.2	16.8
z2	3.2	99	0.2	76.0	0.6	0.275	0.001722 (3.4)	0.0110	0.04634 (3.7)	11.1	11.1	15.4
z3	1.7	106	0.1	42.9	0.6	0.249	0.001237 (8.1)	0.0079	0.04609 (8.6)	8.0	7.9	2.4
z4	4.6	67	0.1	43.3	1.1	0.318	0.001300 (8.0)	0.0083	0.04629 (7.2)	8.4	8.4	13.0

Notes: Mass fractionation correction of 0.15%/amu ± 0.04%/amu (atomic mass unit) was applied to single-collector Daly analyses and 0.12%/amu ± 0.04% for dynamic Faraday-Daly analyses; total procedural blank less than 0.6 pg for Pb and less than 0.1 pg for U; blank isotopic composition: $^{206}Pb/^{204}Pb$ = 19.10 ± 0.1. $^{207}Pb/^{204}Pb$ =15.71 ± 0.1. $^{208}Pb/^{204}Pb$ = 38.65 ± 0.1; age calculations are based on the decay constants of Steiger and Jäger (1977); common-Pb corrections were calculated by using the model of Stacey and Kramers (1975) and the interpreted age of the sample; GDCC = Cascada granodiorite

[1] Sample weights are estimated by using a video monitor and are known to within 40%

[2] Total common-Pb in analyses

[3] Measured ratio corrected for spike and fractionation only

[4] Radiogenic Pb

[5] Corrected for fractionation. spike. blank. and initial common Pb

Appendix 3. Summary of SHRIMP U-Pb Zircon Results for the Dacite Plug

							Total				Radiogenic			
Grain. spot	U (ppm)	Th (ppm)	Th/U	$^{206}Pb^*$ (ppm)	$^{204}Pb/^{206}Pb$	f_{206} (%)	$^{238}U/^{206}Pb$	±	$^{207}Pb/^{206}Pb$	±	$^{206}Pb/^{238}U$	±	$^{206}Pb/^{238}U$	Age (Ma) ±
1.1	547	421	0.77	0.4	–0.007030	9.41	1138.6	27.4	0.1205	0.0099	0.00080	0.00002	5.13	0.16
2.1	233	190	0.81	0.2	0.024551	14.40	938.2	32.4	0.1599	0.0147	0.00091	0.00004	5.88	0.27
2.2	745	596	0.80	0.5	0.014071	11.17	1209.5	36.4	0.1343	0.0124	0.00073	0.00003	4.73	0.18
2.3	696	476	0.68	0.5	0.001697	9.49	1158.2	36.6	0.1211	0.0086	0.00078	0.00003	5.04	0.18
3.1	453	269	0.59	0.3	0.006084	5.26	1248.2	36.7	0.0876	0.0094	0.00076	0.00002	4.89	0.16
4.1	570	346	0.61	0.4	0.009331	7.91	1212.3	28.9	0.1086	0.0108	0.00076	0.00002	4.89	0.15
5.1	522	426	0.82	0.3	0.006732	6.98	1283.0	37.0	0.1013	0.0096	0.00073	0.00002	4.67	0.15
5.2	13	4	0.32	0.0	0.120305	90.14	266.6	20.5	0.7580	0.0840	0.00037	0.00059	2.38	3.77
6.1	432	198	0.46	0.3	0.009970	7.13	1203.2	32.0	0.1025	0.0096	0.00077	0.00002	4.97	0.16
7.1	655	552	0.84	0.5	-	8.87	1237.5	29.7	0.1162	0.0115	0.00074	0.00002	4.75	0.15
8.1	506	355	0.70	0.4	0.008594	6.45	1152.0	36.7	0.0971	0.0117	0.00081	0.00003	5.23	0.19
9.1	636	600	0.94	0.5	-	5.22	1198.2	26.7	0.0873	0.0064	0.00079	0.00002	5.10	0.13
1.01	557	668	1.20	0.4	-	6.31	1206.8	29.1	0.0960	0.0099	0.00078	0.00002	5.00	0.14
11.1	423	206	0.49	0.3	0.013020	9.35	1284.9	35.2	0.1200	0.0191	0.00071	0.00003	4.55	0.18
12.1	419	269	0.64	0.3	-	8.97	1203.0	32.3	0.1170	0.0101	0.00076	0.00002	4.88	0.16
13.1	410	296	0.72	2.3	0.002772	2.09	153.9	2.1	0.0634	0.0048	0.00636	0.00010	40.87	0.61
14.1	463	335	0.72	0.3	0.017936	8.55	1151.8	28.7	0.1137	0.0144	0.00079	0.00003	5.12	0.17
15.1	510	265	0.52	0.4	0.005144	8.62	1054.5	24.9	0.1143	0.0187	0.00087	0.00003	5.58	0.21
16.1	2039	705	0.35	48.1	0.000037	0.23	36.4	0.7	0.0514	0.0005	0.02741	0.00051	174.29	3.20
16.2	643	471	0.73	0.5	0.008107	12.24	1118.7	24.5	0.1428	0.0172	0.00078	0.00003	5.05	0.19
17.1	490	340	0.69	0.3	-	8.87	1243.5	31.2	0.1162	0.0088	0.00073	0.00002	4.72	0.14
18.1	344	231	0.67	0.3	0.023429	14.07	1141.9	33.9	0.1573	0.0128	0.00075	0.00003	4.85	0.20
		Age		± no std		± include std								
		4.916		0.091		0.100								

Notes: Uncertainties given at the 1σ level; error in FC1 Reference zircon calibration was 0.82% for the analytical session (not included in above errors but required when comparing data from different mounts); f_{206} % denotes the percentage of ^{206}Pb that is common Pb; * = radiogenic; - = no data; correction for common Pb made using the measured $^{238}U/^{206}Pb$ and $^{207}Pb/^{206}Pb$ ratios following Tera and Wasserburg (1972) as outlined in Compston et al. (1992)

Appendix 4. $^{40}Ar/^{39}Ar$ Analytical Data for Biotite Incremental Step-Heating and Vein Spot Fusion

No. step	Temperature		$^{36}Ar(a)$	$^{37}Ar(ca)$	$^{38}Ar(cl)$	$^{39}Ar(k)$	$^{40}Ar(r)$	Age (Ma)	$\pm 2\sigma$ (Ma)	$^{40}Ar(r)$ (%)	$^{39}Ar(k)$ (%)	K/Ca	$\pm 2\sigma$
GDRB-1 - DDH173 (223 m); biotite (250–500 μm) J value: 0.001608													
1	600°C		0.00000	0.00123	0.00001	0.00043	0.00925	61.60	± 17.97	99.95	0.10	0.150	± 0.130
2	800°C		0.00016	0.00064	0.00013	0.00843	0.05201	17.81	± 8.40	52.44	1.90	5.627	± 7.130
3	900°C	×	0.00018	0.00110	0.00045	0.02372	0.09426	11.49	± 2.93	63.45	5.36	9.297	± 6.848
4	1000°C	×	0.00011	0.00051	0.00111	0.04948	0.19013	11.11	± 1.44	84.96	11.17	41.496	± 66.358
5	1100°C	×	0.00004	0.00073	0.00143	0.06869	0.26065	10.97	± 1.09	95.74	15.51	40.382	± 47.535
6	1200°C	×	0.00005	0.00000	0.00171	0.07309	0.27575	10.91	± 0.56	94.29	16.50	0.00007	± 0.00
7	1300°C	×	0.00004	0.00076	0.00172	0.06913	0.26417	11.05	± 0.71	95.59	15.61	38.859	± 13.965
8	1375°C	×	0.00001	0.00062	0.00159	0.06941	0.26455	11.02	± 0.58	98.96	15.67	48.500	± 21.360
9	1450°C	×	0.00001	0.00100	0.00183	0.08049	0.30334	10.90	± 0.77	98.77	18.17	34.629	± 7.655
		∑	0.00060	0.00659	0.00998	0.44287	1.71413						
GDRB-2 - DDH173 (30 m); biotite (425–500 μm) J value: 0.001739													
1	500°C		0.00052	0.00030	0.00018	0.00268	0.03175	36.73	± 5.69	17.15	0.15	3.908	± 2.204
2	700°C	×	0.00099	0.00103	0.00102	0.02560	0.09145	11.17	± 1.24	23.81	1.39	10.738	± 1.269
3	900°C	×	0.00217	0.00386	0.00926	0.23831	0.88386	11.60	± 0.17	57.96	12.91	26.561	± 1.466
4	1000°C	×	0.00100	0.00362	0.01032	0.27634	1.03567	11.72	± 0.12	77.80	14.96	32.865	± 2.127
5	1100°C	×	0.00121	0.00534	0.01380	0.37176	1.38974	11.69	± 0.12	79.57	20.13	29.932	± 1.239
6	1200°C	×	0.00080	0.00602	0.01387	0.37684	1.39020	11.54	± 0.08	85.49	20.41	26.905	± 1.454
7	1300°C	×	0.00075	0.00620	0.01282	0.33995	1.25060	11.50	± 0.15	84.92	18.41	23.584	± 0.929
8	1400°C	×	0.00050	0.00567	0.00793	0.21513	0.78647	11.43	± 0.19	84.12	11.65	16.311	± 0.701
		∑	0.00793	0.03203	0.06920	1.84661	6.85973						
Diorite - DDH742 (106.5 m); bioite (250–300 μm) J value: 0.001582													
1	400°C		0.00009	0.00009	0.00004	0.00014	0.00233	47.09	± 146.98	7.87	0.03	0.646	± 0.730
2	600°C		0.00006	0.00006	0.00003	0.00083	0.01134	38.60	± 31.31	39.56	0.20	6.090	± 10.195
3	750°C	×	0.00016	0.00112	0.00017	0.01144	0.02368	5.90	± 1.87	33.95	2.80	4.390	± 0.452
4	875°C	×	0.00024	0.00156	0.00060	0.03423	0.05601	4.66	± 0.80	43.79	8.37	9.431	± 0.667
5	975°C	×	0.00013	0.00126	0.00065	0.03989	0.06518	4.66	± 0.42	63.06	9.76	13.620	± 1.680
6	1100°C	×	0.00011	0.00179	0.00115	0.06458	0.10553	4.66	± 0.37	75.62	15.79	15.518	± 0.970
7	1200°C	×	0.00010	0.00165	0.00136	0.07716	0.12544	4.63	± 0.15	80.03	18.87	20.112	± 1.734
8	1300°C	×	0.00010	0.00140	0.00107	0.06160	0.09799	4.53	± 0.50	77.30	15.07	18.897	± 1.774
9	1375°C	×	0.00010	0.00133	0.00115	0.06131	0.09726	4.52	± 0.58	76.74	15.00	19.844	± 3.153
10	1400°C	×	0.00010	0.00170	0.00095	0.04892	0.07571	4.41	± 0.27	71.74	11.96	12.373	± 1.352
11	1450°C		0.00007	0.00069	0.00015	0.00878	0.00345	1.12	± 1.23	13.88	2.15	5.474	± 1.146
		∑	0.00126	0.01265	0.00732	0.40889	0.66392						
PQM-1 - DDH577 (28.7 m); biotite (0.5–1 mm) J value: 0.001601													
1	400°C		0.00070	0.00007	0.00001	0.00033	0.01845	152.73	± 41.54	8.21	0.03	2.122	± 2.848
2	600°C		0.00050	0.00170	0.00009	0.00602	0.02007	9.60	± 3.63	11.94	0.50	1.527	± 0.091
3	700°C		0.00048	0.00206	0.00024	0.01755	0.02468	4.06	± 1.06	14.70	1.46	3.662	± 0.135
4	800°C	×	0.00154	0.00260	0.00091	0.06341	0.11117	5.06	± 0.45	19.60	5.28	10.486	± 0.317
5	900°C	×	0.00104	0.00329	0.00224	0.14234	0.23693	4.80	± 0.20	43.31	11.86	18.614	± 0.661
6	1000°C	×	0.00028	0.00264	0.00228	0.13883	0.23571	4.90	± 0.28	73.63	11.57	22.623	± 1.993
7	1100°C	×	0.00017	0.00241	0.00225	0.14013	0.23693	4.88	± 0.24	81.74	11.67	25.028	± 1.256
8	1200°C	×	0.00020	0.00404	0.00259	0.17102	0.27713	4.67	± 0.17	82.06	14.25	18.208	± 1.215
9	1275°C	×	0.00023	0.00564	0.00264	0.16130	0.26267	4.70	± 0.19	79.25	13.44	12.295	± 0.564
10	1350°C	×	0.00019	0.00495	0.00332	0.20260	0.33088	4.71	± 0.17	85.07	16.88	17.598	± 0.748
11	1425°C	×	0.00023	0.00476	0.00262	0.15685	0.24994	4.60	± 0.32	78.50	13.07	14.169	± 0.578
		Σ	0.00557	0.03415	0.01920	1.20038	2.00456						
PQM-2 - DDH231 (155 m); biotite (180–250 μm) J value: 0.001733													
1	500°C	×	0.00068	0.00046	0.00030	0.00897	0.01883	6.55	± 1.93	8.53	0.90	8.340	± 2.066
2	700°C	×	0.00113	0.00220	0.00105	0.06103	0.10292	5.27	± 0.32	23.59	6.16	11.916	± 0.736
3	900°C	×	0.00157	0.00241	0.00333	0.21660	0.35592	5.13	± 0.25	43.42	21.85	38.598	± 2.354
4	1000°C	×	0.00038	0.00076	0.00198	0.13064	0.21700	5.19	± 0.23	65.61	13.18	73.486	± 13.890
5	1100°C	×	0.00040	0.00090	0.00285	0.18627	0.31094	5.21	± 0.11	72.29	18.79	89.262	± 11.563
6	1200°C	×	0.00035	0.00080	0.00276	0.17743	0.28869	5.08	± 0.10	73.35	17.90	94.929	± 20.270
7	1300°C	×	0.00032	0.00081	.00247	0.15884	0.25529	5.02	± 0.13	72.76	16.02	84.705	± 14.932
8	1400°C	×	0.00011	0.00029	0.00081	0.05149	0.08414	5.10	± 0.45	72.79	5.19	75.519	± 35.949
		∑	0.00495	0.00864	0.01556	0.99126	1.63373						

APPENDIX 4. *(Cont.)*

No. step	Temperature		^{36}Ar(a)	^{37}Ar(ca)	^{38}Ar(cl)	^{39}Ar(k)	^{40}Ar(r)	Age (Ma)	±2σ (Ma)	^{40}Ar(r) (%)	^{39}Ar(k) (%)	K/Ca	±2σ
PF – DDH738 (276 m); biotite (0.5–1 mm) J value: 0.001591													
1	400°C		0.00049	0.00008	0.00010	0.00045	0.01640	100.65	± 57.50	10.21	0.02	2.426	± 1.814
2	600°C		0.00049	0.00078	0.00008	0.00799	0.01225	4.39	± 1.99	7.79	0.43	4.406	± 0.542
3	700°C		0.00057	0.00147	0.00038	0.03016	0.04627	4.40	± 0.85	21.42	1.61	8.809	± 0.468
4	800°C	×	0.00071	0.00229	0.00131	0.10511	0.17160	4.68	± 0.20	44.96	5.61	19.757	± 1.288
5	900°C	×	0.00048	0.00224	0.00207	0.17966	0.29087	4.64	± 0.14	67.11	9.60	34.539	± 1.956
6	1000°C	×	0.00032	0.00217	0.00287	0.23939	0.38309	4.59	± 0.10	79.97	12.79	47.543	± 1.775
7	1100°C	×	0.00023	0.00206	0.00334	0.26006	0.42210	4.65	± 0.12	85.76	13.89	54.163	± 2.633
8	1200°C	×	0.00030	0.00410	0.00459	0.37523	0.60527	4.62	± 0.09	86.65	20.04	39.337	± 1.637
9	1300°C	×	0.00032	0.00694	0.00470	0.37903	0.60941	4.61	± 0.11	85.95	20.24	23.483	± 0.856
10	1375°C	×	0.00018	0.00617	0.00251	0.20461	0.33057	4.63	± 0.16	85.77	10.93	14.255	± 0.533
11	1450°C	×	0.00014	0.01225	0.00137	0.09069	0.14587	4.61	± 0.26	77.93	4.84	3.184	± 0.119
		∑	0.00422	0.04055	0.02332	1.87239	3.03370						
PDL stock - DDH746 (302 m); biotite (300–500 μm) J value: 0.001577													
1	600°C		0.00027	0.00027	0.00000	0.00127	0.03802	83.43	± 33.00	32.24	0.31	2.028	± 4.350
2	800°C		0.00048	0.00080	0.00013	0.01754	0.07673	12.40	± 1.66	35.31	4.33	9.412	± 6.708
3	900°C	×	0.00062	0.00125	0.00031	0.05216	0.08691	4.73	± 1.17	32.23	12.87	17.924	± 9.073
4	1000°C	×	0.00028	0.00049	0.00046	0.05644	0.09899	4.98	± 0.83	54.15	13.92	49.897	± 102.080
5	1100°C	×	0.00017	0.00044	0.00042	0.04926	0.08304	4.79	± 1.07	61.74	12.15	48.565	± 110.868
6	1200°C	×	0.00011	0.00035	0.00038	0.04089	0.07038	4.89	± 1.09	68.87	10.09	49.719	± 136.426
7	1275°C	×	0.00012	0.00098	0.00043	0.05094	0.08546	4.77	± 0.77	70.07	12.57	22.255	± 21.207
8	1350°C	×	0.00011	0.00076	0.00043	0.06807	0.11410	4.76	± 1.26	77.67	16.79	38.501	± 43.004
9	1400°C	×	0.00009	0.00102	0.00040	0.05527	0.09065	4.66	± 2.27	76.42	13.64	23.358	± 18.706
10	1425°C	×	0.00000	0.00073	0.00001	0.01352	0.02773	5.83	± 5.84	95.45	3.33	8.002	± 10.025
		∑	0.00225	0.00709	0.00296	0.40536	0.77202						
PDL stock duplicate - DDH746 (302 m); biotite (150–180 μm) J value: 0.001741													
1	400°C		0.00038	0.00000	0.00005	0.00301	0.01540	16.02	± 11.04	12.10	0.12	0.000	± 0.000
2	600°C	×	0.00168	0.00076	0.00040	0.05085	0.07011	4.33	± 0.72	12.39	2.10	28.592	± 9.144
3	700°C	×	0.00255	0.00108	0.00102	0.13415	0.20030	4.68	± 0.35	20.95	5.55	53.288	± 10.514
4	800°C	×	0.00254	0.00103	0.00141	0.18605	0.27383	4.62	± 0.21	26.69	7.70	77.359	± 16.695
5	900°C	×	0.00267	0.00099	0.00239	0.31531	0.46526	4.63	± 0.23	37.03	13.05	136.469	± 30.018
6	975°C	×	0.00127	0.00092	0.00188	0.25608	0.38534	4.72	± 0.17	50.57	10.60	119.320	± 35.735
7	1050°C	×	0.00084	0.00092	0.00150	0.20559	0.29954	4.57	± 0.17	54.53	8.51	96.076	± 21.603
8	1125°C	×	0.00091	0.00104	0.00182	0.22917	0.32872	4.50	± 0.13	54.91	9.49	94.714	± 28.125
9	1200°C	×	0.00090	0.00188	0.00200	0.25992	0.38813	4.68	± 0.15	59.20	10.76	59.414	± 8.375
10	1250°C	×	0.00100	0.00222	0.00207	0.27122	0.39663	4.59	± 0.17	57.14	11.23	52.603	± 7.773
11	1300°C	×	0.00104	0.00278	0.00204	0.27453	0.39090	4.47	± 0.13	55.75	11.36	42.388	± 4.192
12	1400°C	×	0.00096	0.00213	0.00172	0.22979	0.32550	4.44	± 0.17	53.22	9.51	46.415	± 5.162
		Σ	0.01672	0.01577	0.01831	2.41566	3.53966						
GDCC - DDH735 (200 m); quartz-sericite vein J value: 0.00164													
1	1400°C	×	0.00964	0.13164	0.00401	0.22533	0.37013	4.85	± 0.55	11.49	29.26	0.736	± 0.036
2	1400°C	×	0.00052	0.03285	0.00037	0.11297	0.17099	4.47	± 0.18	52.66	14.67	1.479	± 0.073
3	1400°C	×	0.00053	0.02618	0.00050	0.14876	0.21658	4.30	± 0.39	57.65	19.32	2.443	± 0.122
4	1400°C	×	0.00032	0.01129	0.00024	0.10683	0.15437	4.27	± 0.43	61.46	13.87	4.067	± 0.233
5	1400°C	×	0.00106	0.08347	0.00053	0.17627	0.25555	4.28	± 0.21	44.85	22.89	0.908	± 0.048
		∑	0.01208	0.28543	0.00566	0.77015	1.16762						
PDL - DDH746 (37.5 m); quartz-sericite vein J value: 0.001664													
1	1400°C		0.01168	0.02216	0.00075	0.21595	0.43939	6.10	± 0.53	11.29	11.32	4.190	± 0.207
2	1400°C	×	0.00053	0.01111	0.00014	0.15368	0.21697	4.23	± 0.20	58.03	8.05	5.947	± 0.317
3	1400°C	×	0.00091	0.04191	0.00044	0.50771	0.73251	4.33	± 0.06	72.71	26.61	5.210	± 0.259
4	1400°C	×	0.00058	0.03080	0.00044	0.38139	0.56008	4.40	± 0.05	76.09	19.99	5.325	± 0.262
5	1400°C	×	0.00032	0.02031	0.00024	0.22288	0.32047	4.31	± 0.09	76.91	11.68	4.718	± 0.242
6	1400°C	×	0.00037	0.02832	0.00004	0.30714	0.45277	4.42	± 0.06	79.90	16.10	4.664	± 0.235
7	1400°C		0.00025	0.01334	0.00001	0.11926	0.14446	3.63	± 0.35	66.04	6.25	3.843	± 0.219
		∑	0.01464	0.16795	0.00206	1.90803	2.86665						

Appendix 4. *(Cont.)*

No. step	Temperature		^{36}Ar(a)	^{37}Ar(ca)	^{38}Ar(cl)	^{39}Ar(k)	^{40}Ar(r)	Age (Ma)	±2σ (Ma)	^{40}Ar(r) (%)	^{39}Ar(k) (%)	K/Ca	±2σ
GDCC - DDH735 (194.3 m); K-feldspar vein J value: 0.001713													
1	1400°C		0.03859	0.03893	0.01301	0.37689	1.73506	14.17	± 1.36	13.20	42.46	4.163	± 0.195
2	1400°C	×	0.00036	0.00248	0.00017	0.04152	0.07200	5.35	± 0.51	40.43	4.68	7.194	± 1.423
3	1400°C	×	0.00088	0.00770	0.00051	0.14191	0.24200	5.26	± 0.22	48.00	15.99	7.924	± 0.468
4	1400°C	×	0.00058	0.00641	0.00034	0.11126	0.18968	5.26	± 0.21	52.57	12.53	7.468	± 0.517
5	1400°C	×	0.00051	0.00532	0.00034	0.09568	0.15581	5.03	± 0.39	50.60	10.78	7.728	± 0.644
6	1400°C	×	0.00057	0.00704	0.00032	0.12041	0.20871	5.35	± 0.35	55.17	13.56	7.357	± 0.441
		∑	0.04149	0.06788	0.01470	0.88767	2.60325						
BXMGD - TSS22 (802 m); K-feldspar vein J value: 0.001692													
1	1400°C		0.08529	0.02443	0.01306	0.53000	2.73569	15.69	± 2.63	9.79	29.26	9.330	± 0.705
2	1400°C	×	0.00181	0.00429	0.00062	0.19623	0.30587	4.75	± 0.16	36.26	10.83	19.663	± 1.826
3	1400°C	×	0.00184	0.00565	0.00095	0.36847	0.56664	4.69	± 0.16	50.92	20.34	28.021	± 1.838
4	1400°C	×	0.00076	0.00301	0.00048	0.20362	0.30104	4.51	± 0.13	57.00	11.24	29.115	± 2.872
5	1400°C	×	0.00200	0.00279	0.00066	0.35549	0.55601	4.77	± 0.15	48.34	19.63	54.713	± 7.119
6	1400°C	×	0.00048	0.00251	0.00027	0.15734	0.24313	4.71	± 0.42	62.99	8.69	27.008	± 4.054
		∑	0.09218	0.04268	0.01605	1.81115	4.70837						
GDCC - DDH728 (163.8 m); biotite vein J value: 0.001736													
1	1400°C		0.03073	0.03923	0.00891	0.20979	0.79942	11.90	± 1.47	8.09	20.55	2.300	± 0.105
2	1400°C	×	0.00104	0.01206	0.00187	0.12018	0.16904	4.40	± 0.38	35.40	11.77	4.287	± 0.238
3	1400°C	×	0.00048	0.00838	0.00135	0.09418	0.13900	4.62	± 0.45	49.21	9.23	4.834	± 0.260
4	1400°C	×	0.00046	0.00885	0.00147	0.10298	0.14800	4.50	± 0.30	51.88	10.09	5.002	± 0.291
5	1400°C	×	0.00178	0.01410	0.00258	0.16052	0.24268	4.73	± 0.23	31.53	15.73	4.897	± 0.260
6	1400°C	×	0.00037	0.01779	0.00247	0.19439	0.28690	4.62	± 0.20	71.89	19.04	4.698	± 0.251
7	1400°C	×	0.00025	0.01432	0.00198	0.13870	0.20021	4.52	± 0.25	72.39	13.59	4.165	± 0.231
		∑	0.03511	0.11472	0.02062	1.02073	1.98525						
GDCC - DDH728 (163.8 m); biotite vein J value: 0.001759													
1	1400°C		0.00301	0.01890	0.00103	0.04525	0.09486	6.64	± 1.10	9.64	8.92	1.029	± 0.050
2	1400°C	×	0.00180	0.03412	0.00134	0.06596	0.10940	5.26	± 0.66	17.03	13.00	0.831	± 0.040
3	1400°C	×	0.00051	0.01998	0.00087	0.05121	0.08346	5.16	± 0.37	35.49	10.10	1.102	± 0.054
4	1400°C		0.00156	0.02577	0.00092	0.05158	0.11699	7.18	± 0.45	20.27	10.17	0.861	± 0.041
5	1400°C	×	0.00026	0.01169	0.00047	0.02655	0.04713	5.62	± 0.88	38.20	5.23	0.977	± 0.056
6	1400°C	×	0.00039	0.01825	0.00064	0.03689	0.06581	5.65	± 0.63	36.13	7.27	0.869	± 0.043
7	1400°C		0.00771	0.09550	0.00256	0.15165	0.33390	6.97	± 0.65	12.78	29.90	0.683	± 0.042
8	1400°C		0.00513	0.05617	0.00119	0.07811	0.16697	6.77	± 0.78	9.91	15.40	0.598	± 0.037
		∑	0.02036	0.28039	0.00902	0.50720	1.01852						

× = steps used for age calculations; abbreviations: (a) = atmospheric, (ca) = calcium, (cl) = chlorine, (k) = potassium, and (r) = radiogenic